Concerted Up-regulation of Aldehyde/Alcohol Dehydrogenase (ADHE) and Starch in Chlamydomonas reinhardtii Increases Survival under Dark Anoxia

Robert van Lis, Marion Popek, Yohann Couté, Artemis Kosta, Dominique Drapier, Wolfgang Nitschke, Ariane Atteia

Concerted upregulation of bifunctional aldehyde/alcohol dehydrogenase (ADHE) and starch content in *Chlamydomonas* cells allows increased survival in prolonged dark anoxia.

Robert van Lis[1,2], Marion Popek[1], Yohann Couté[3,4,5], Artemis Kosta[6], Dominique Drapier[7], Wolfgang Nitschke[1] and Ariane Atteia[1,†]

[1]Aix Marseille Univ, CNRS, the Unité de Bioénergétique et Ingénierie des Protéines-UMR 7281, 31 Chemin Joseph Aiguier, F-13402 Marseille, France
[2]INRA, Laboratoire de Biotechnologie de l'Environnement, Narbonne, France
[3]Université Grenoble Alpes, BIG-BGE, F-38000 Grenoble, France
[4]Commissariat à l'Energie Atomique, BIG-BGE, F-38000 Grenoble, France
[5]INSERM, BGE, F-38000 Grenoble, France
[6]Microscopy core facility, FR3479 Institut de Microbiologie de la Méditerranée 31 chemin Joseph Aiguier, 13402 Marseille cedex 20, France
[7]Institut de Biologie Physico-Chimique, UMR7141 CNRS-UPMC, Paris, 75005, France.

Running title: *Chloroplast aldehyde/alcohol dehydrogenase*

[†]To whom correspondence should be sent : Aix Marseille Univ, CNRS, the Unité de Bioénergétique et Ingénierie des Protéines-UMR 7281, 31 Chemin Joseph Aiguier, F-13402 Marseille, France. E-mail: ariane.atteia@imm.cnrs.fr

Keywords: Algae, *Chlamydomonas*, fermentation, metalloprotein, metabolism, regulation,
For the website: ADH, *Chlamydomonas*, chloroplast, microscopy, western blots

ABSTRACT

Aldehyde/alcohol dehydrogenases (ADHEs) are bifunctional enzymes which commonly produce ethanol from acetyl-CoA with acetaldehyde as intermediate, and play a key role in anaerobic redox balance in many fermenting bacteria. Herein we provide the first molecular and enzymatic characterization of the ADHE from a photosynthetic organism, the microalga *Chlamydomonas reinhardtii*. Purified recombinant enzyme catalyses the reversible NADH-mediated interconversions of acetyl-CoA, acetaldehyde and ethanol, but seems to be poised towards the production of ethanol from acetaldehyde. Phylogenetic analysis supports a cyanobacterial origin for the *Chlamydomonas* enzyme. In the chloroplast stroma, native ADHE associates in dimers and higher order oligomers. Analysis of ADHE-enriched stromal fractions by electron microscopy revealed the presence of fine spiral structures, similar to bacterial ADHE spirosomes. Protein blots showed that ADHE abundance is regulated under oxic conditions, and is induced in cells exposed to diverse physiological stresses, including zinc-deficiency, nitrogen starvation and inhibition of carbon concentration/fixation capacity. Analyses of the overall proteome and fermentation profiles reveal that cells with increased ADHE abundance exhibit a higher capacity to survive under dark anoxia. This likely relates to the fact that enhanced ADHE content appears to coincide with enhanced starch accumulation, which could be viewed as an anticipation of ADHE-mediated anaerobic survival.

INTRODUCTION

Photosynthetic microorganisms are typically associated with illuminated oxic environments, and so little attention is paid to energy generation in conditions of dark anoxia. The study of the anaerobic heterotrophic metabolism of both microalgae and cyanobacteria is however highly relevant since these organisms regularly face conditions of dark anoxia in their natural habitats in the dark (or on cloudy days), especially in polluted environments. In order to meet the energy demand for life or cell maintenance in these specific conditions, photosynthetic cells carry out fermentation at the expense of endogenous carbohydrates (glycogen or starch). Anaerobic respiration has also been reported, *i.e.* sulfur respiration in cyanobacterial species such as *Oscillatoria limnetica* and *Microcoleus chthonoplastes*, (1,2), and fumarate respiration in *Euglena gracilis* (3,4).

In cyanobacteria, the fermentation routes are diverse, and include homofermentation (lactate or acetate), heterofermentation and mixed-acid fermentation (5). Among microalgae, fermentative metabolism has been investigated mainly in chlorophytes. It is known for some time that in absence of oxygen, green algae such as *Chlamydomonas* and *Chlorella* have the ability to produce organic acids (acetate, formate, lactate, succinate), alcohols (ethanol) and gases (CO_2, H_2) (6-9). The genome sequences of *Chlamydomonas reinhardtii* (10) and *Chlorella variabilis* NC64 (11) have greatly helped to get a good grasp of the anaerobic pathways in the two algae (12-14). Since then, in *C. reinhardtii*, henceforth called *Chlamydomonas*, these pathways have been actively investigated through molecular and biochemical studies of the fermentative enzymes (15-19) as well as physiological studies of mutant strains (20-25). As we understand it, the "core" anaerobic network in the chlorophyte combines enzymes commonly found in eukaryotes, *i.e.* pyruvate decarboxylase (PDC), alcohol dehydrogenases (ADH) and lactate dehydrogenase (LDH), with enzymes that are typical for bacteria (referred to as bacterial-type enzymes), *i.e.* pyruvate formate lyase (PFL; EC 2.3.1.54), pyruvate:ferredoxin oxidoreductase (PFO or PFR; EC 1.2.7.1), iron-only hydrogenases (Fe-HYD), and aldehyde/alcohol dehydrogenase (ADHE, or ADH1) (Fig. 1). The presence of these bacterial-type enzymes raises questions about their evolutionary origin and their integration in a mitochondriate eukaryote that we and others have tackled since their discovery. PFL and PFO were both shown to be functional in *Chlamydomonas* (16, 18, 19) and can under anaerobic conditions catalyze the production of acetyl-CoA from pyruvate. PFL accumulates under aerobic conditions and is dually targeted to chloroplast and mitochondria (12). PFO is expressed under anaerobic conditions and localizes to the chloroplast where it is coupled to H_2 production by Fe-HYD via FDX1 (PetF) (18, 19). ADHE is a mono-iron enzyme, which was

found to be the major ethanol-producing enzyme in conditions of dark anoxia (22). Although it is now clear that the bacterial-type enzymes fully participate in the anaerobic life of *Chlamydomonas*, their physiological significance in the intricate anaerobic network (Fig. 1) as well as their regulation remain largely enigmatic.

To better understand the integration and the regulation of the ADHE in the context of a photosynthetic eukaryotic cell, we explored different aspects of *Chlamydomonas* ADHE, in particular its evolutionary origin, subcellular localization, enzymatic properties and its integration in cellular metabolism. In this study we also investigated the physiological regulation of ADHE in the alga. This is the first report on the factors that influence the ADHE abundance in *Chlamydomonas* and on the consequences of enhanced levels in fermentation behaviour.

RESULTS

Phylogenetic analyses of Chlamydomonas ADHE - ADHE genes are present in the five eukaryotic supergroups described by Adl et al. (2012)(26) , *i.e.* the Archaeplastida, Amoebozoa, Excavates, Opisthokonta and the Stramenopiles-Alveolata-Rhizaria (SAR) (Table 1). Yet, the gene remains poorly represented amongst eukaryotes, where it appears to be restricted to unicellular species, most of which are pathogenic anaerobes. The only free-living eukaryotes in which an ADHE gene has been found so far are microalgae. Besides the chlorophytes *Chlamydomonas*, *Chlorella*, and *Polytomella* (Archaeplastida), an ADHE gene is also present in two photosynthetic species of the SAR supergroup, the cryptophyte *Guillardia theta* and the chlorarachniophyte *Bigelowiella natans* (14) (Table 1).

Earlier phylogenies have shown most eukaryotic ADHEs wedged in between two clusters of bacterial enzymes (27). The ADHE phylogenetic analysis that we present here includes a significantly larger set of bacterial sequences as well as all eukaryotic sequences publicly available (Supplemental Data Sets 1, 2). The current analysis further substantiates the dichotomy of the bacterial ADHEs (clusters I and II) and the unclear rooting of most eukaryote proteins (Fig. 2). The ADHEs from the marine algae *B. natans* and *G. theta* are found in the undefined "eukaryotic" region of the tree, while the enzymes of *Chlamydomonas* and other chlorophytes are found in cluster I, where they branch with cyanobacterial ADHEs (Fig. 2). Our phylogenetic analysis thus suggests that *i*) the origin of the chlorophyte enzymes is distinct from that of the other eukaryotic enzymes and *ii*) the ADHE gene in green algae might have been inherited vertically from the cyanobacterial ancestor.

The unique phylogenetic position of *Chlamydomonas* ADHE compared to that of the eukaryotic enzymes studied so far, *i.e. Entamoeba* (Amoebozoa) (28-29) and *Giardia* (Excavata) (30), was a motive to study in detail its biochemical characteristics and its regulation.

Subcellular localization and oligomerization of Chlamydomonas ADHE - Relative to bacterial ADHEs, the *Chlamydomonas* 954 aa-protein exhibits an extended N-terminus (~60 residues) (Fig. 3A), which could serve as an intracellular targeting signal to the chloroplast and/or the mitochondrion. The targeting of ADHE to the bioenergetic organelles was evaluated by protein blots using antibodies raised against a truncated form of the algal ADHE (tADHE, Val354-Pro703) (12). These antibodies recognize native ADHE with an apparent molecular mass of ~100 kDa (Fig. 4A). To isolate chloroplasts and mitochondria, we used mutant strain 10-6C, in which ADHE abundance was found to be 3-4 fold higher than in wild-type strain CC-124 (Supplemental Fig. S1). Strain 10-6C is a photosynthetic mutant impaired in CO_2 assimilation due to a point mutation in the *rbcL* gene (31,32) (Supplemental Fig. S2). The relative purity of the organelle fractions was evaluated with antibodies against the light harvesting complex proteins (LHCs) and subunit beta of mitochondrial F_0F_1-ATPase (ATP2). Immunoblot analysis indicated that ADHE is present in the chloroplast fraction but not in the fraction enriched in mitochondria (Fig. 3A). Our result, obtained with cells grown under oxic conditions, thus corroborates proteomics data on organelles isolated from anaerobic cells (33). *Chlamydomonas* is the first organism for which an ADHE chloroplast location is found. Indeed, ADHE was so far described in the cytosol of parasites such as *Piromyces* and *Giardia* (4, 34) and in the

mitochondria of the non-photosynthetic chlorophyte *Polytomella* (27).

In order to gain insights into the intra-organellar localization of the ADHE in *Chlamydomonas*, chloroplasts were broken by two freeze-thaw cycles, and fractionated by a low-speed centrifugation. In the resulting supernatant which contains primarily stromal proteins (not shown), the ADHE was identified by mass spectrometry-based proteomic analysis with a coverage of more than 50% over the entire sequence (Supplemental Fig. S3).

To study the oligomerization state of the native ADHE, the enzyme was further purified by anion exchange chromatography and affinity chromatography on Blue Sepharose resin. Assessment of the oligomerization state was done by two-dimensional Blue Native (BN)/SDS-PAGE and immunoblotting. Protein blots showed that ADHE occurred in various complexes of similar abundance (Fig. 4B); the smallest complex of ~180-kDa is likely a dimer, the complex in the range of ~400-kDa might represent a tetramer. PFL, present in the same stromal fraction, was found mainly as a monomer at ~80-kDa and a dimer at ~160-kDa (Fig. 4B). The various ADHE forms observed on BN-PAGE, might be indicative of the protein tendency to aggregate. Alternatively, these different forms might indicate the progressive dissociation of large assemblies during purification and/or migration on the native gel. The possibility that ADHE self-associates as large molecular assemblies in the chloroplast was supported by *i*) the fact that the protein eluted from anion exchange chromatography could be pelleted after ultracentrifugation and *ii*) the presence in the ADHE-containing pellet of spiral-like filaments of an average length of 100 nm (Fig. 4C) that appeared morphologically indistinguishable from bacterial ADHE oligomers, also known as spirosomes (35-37). Our attempts to obtain samples enriched in these filaments by either centrifugation on concentrating devices or ammonium sulfate precipitation have failed, suggesting that *Chlamydomonas* spirosomes are relatively fragile.

Molecular characterization and kinetic analysis of recombinant ADHE - Considering the low amounts of ADHE present in *Chlamydomonas*, even in strain 10-6C, we chose to study the recombinant enzyme. The ADHE gene was cloned into the pET24a vector and the protein expressed in *E. coli*. A hexahistidine tag added to the C-terminus of the ADHE allowed fast purification via affinity chromatography on a Ni-column (Fig. 5A).

The oligomeric state of freshly purified rADHE was first assessed by gel filtration. The elution profile in 50 mM potassium phosphate, pH 7.0, supplemented with 150 mM NaCl revealed the heterogeneity of the sample, with different complexes of molecular masses ranging between 200-kDa and 600-kDa (not shown). On BN-gel, rADHE was resolved as several bands (Fig. 5B): one major complex of ~180-kDa, a complex of ~500-kDa, and several minor bands at lower (<120 kDa) and higher molecular mass range (> 669-kDa). This BN profile was reproducible, even when enzyme purification was carried out under atmospheric conditions (Fig. 5B, lane 2). All protein bands, except the lowest at ~90-kDa, showed a NAD^+-dependent alcohol dehydrogenase activity (Fig. 5B). The enzymatically-active complex of ~180 kDa, that runs in the same region as *S. cerevisiae* tetrameric alcohol dehydrogenase (Mr~160-kDa), is likely a dimer. Two-dimensional BN/SDS-PAGE confirmed that rADHE occurs in multiple oligomeric forms, like the native ADHE. But in contrast to the native enzyme, the rADHE associates most predominantly into homodimers (Fig. 5C).

Bifunctional aldehyde/alcohol dehydrogenase consists of an ADH domain and an aldehyde dehydrogenase (ALDH) domain (Fig. 3A). ADHEs typically catalyze the two distinct activities which are reversible (30) (Fig. 3B). Here we first assessed the ability of the purified rADHE enzyme to catalyse each of the four different partial reactions. For the NADH-dependent acetyl-CoA and acetaldehyde reduction activities, the enzyme exhibited Vm values of 1 and 4 U/mg, respectively (Table 2; reactions 1 and 2). Both reductive reactions show highest activities in the pH range of 6.0-7.0 (Table 2). Reductions of acetyl-CoA and acetaldehyde appear specific for NADH, since the Vm for NADPH was only 1-2% of that for NADH (not shown). The specific activities of NAD^+-dependent ethanol and acetaldehyde oxidations were both found to be in the range of 1-1.5 U/mg (reactions 3 and 4) (Table 2). Overall, reaction

2 showed the highest activity, which may represent an adaptation to quickly remove acetaldehyde, a compound toxic for the cell. Also, from the fact that reaction 4 is much lower than reaction 2 it could be hypothesized that the enzyme is poised to function towards the production of ethanol and not vice versa, at least under the saturating conditions used for the measurements. Iron addition to rADHE exhibited a (moderate) stimulating effect on all activities (Table 2) while an incubation in 100 mM in EDTA had no clear inhibitory effect.

The recombinant enzyme rADHE was further characterized for the substrate affinities of its forward reactions (reactions 1 and 2), which are metabolically relevant. Acetyl-CoA reduction (reaction 1) obeyed Michaelis-Menten kinetics with an apparent Km for acetyl-CoA of 12.7 ± 2.9 µM (Table 3). The kinetics of NADH is less clear and likely confounded by the fact that NADH is also used in reaction 2, using the reaction product of reaction 1. A typical Michaelis-Menten curve was obtained for NADH in acetaldehyde reduction (reaction 2) with a Km of 20.9 ± 3.5 µM (Table 3).

Analysis of fermentation products by ADHE overexpression strain- To have insights into the regulation of the carbon fluxes in the green alga, we investigated the fermentative capabilities of strain 10-6C which accumulates ~3.5 times more ADHE than the wild-type strain CC-124. Algal cells were incubated in dark conditions in AIB medium, a standard medium used to study algal fermentation (13). The products excreted by the cells were analysed by HPLC at 0-8 h and at 24 h. Forty-five minutes after the shift to anoxia, formate, ethanol and acetate were already detected in the extracellular medium, and their production continued steadily up to 8 h (Fig. 6). After 8 h of dark anoxia, the formate production by strains CC124 and 10-6C was comparable at about 0.6 mM (1 x 10^7 cells mL^{-1}), indicating that the ADHE-overaccumulating strain catabolizes endogenous carbon reserves in a similar manner (products and kinetics) as the wild-type, *i.e.* pyruvate stemming from glycolysis is directed mostly to pyruvate formate lyase (Fig. 1). When acetyl-CoA produced by PFL is equally distributed between ADHE and PTA/ACK, ethanol and acetate are expected to be produced in equimolar amounts. A balanced production of acetate and ethanol was indeed observed with the WT strain, with 0.34 mM of each product after an incubation of 8 h. In the case of strain 10-6C, the production of acetate appeared somewhat lower than that of ethanol with 0.28 mM and 0.43 mM, respectively (Fig. 6), which suggests a slight shift in the distribution of acetyl-CoA towards ADHE. This imbalance could be explained by the increased ADHE levels in the mutant strain, although the increase in ethanol production (<1.4) is not in proportion with the increase in ADHE abundance (~3.5; Table 4). After 24 h of dark anoxia, the fermentation profiles of the WT strain were comparable to those at 8 h, indicating no further fermentation after 8 h. In contrast, the levels of each product excreted by the mutant strain after 24 h had about doubled relative to 8 h, reaching 1.2 mM formate, 0.5 mM acetate and 0.83 mM ethanol (Fig. 6).

To further investigate the fermentative abilities of strain 10-6C in view of its elevated ADHE levels, we blocked the PFL-gated pathway by adding to the cells the PFL-inhibitor sodium hypophosphite (HP) (16). As shown in Fig. 6, strains CC-124 and 10-6C displayed the same overall response to HP: a production of formate and acetate nearly abolished and a yield of ethanol increased by 1.5-2 fold. The HPLC profiles did not reveal any other metabolites, not even lactate. Thus, irrespective of the strain, ethanol homofermentation is the main (only) route when PFL is blocked, which is likely to proceed via PDC and ADHE (Fig. 1).

The HP-inhibited cells showed the same fermentation trend during extended anoxia as compared to non-inhibited cells, *i.e.* fermentation by strain CC-124 stopped after 6 h but continued in strain 10-6C. The ethanol production by the latter strain almost doubled between 6 h and 24 h, reaching concentrations of 1.75 mM (Fig. 6). Altogether our data indicated that the ADHE-overaccumulating strain exhibits an extended fermentative capacity compared to the wild-type strain, whether PFL is inactivated or not.

Protein levels in dark anoxia - Protein extracts from CC-124 and 10-6C cells exposed to dark anoxia were analyzed by SDS-PAGE. As observed in Fig. 7A, a drastic change in the overall protein profile of wild-type cells was observed between 6 h and 24 h (when fermentation stops). In contrast, protein

profiles of mutant strain 10-6C appeared stable through the 24 h-period. To gain insights into the respective acclimation of the two strains to dark anoxia, selected proteins were followed by immunoblotting experiments (Fig. 7B). For both strains, a slight increase in ADHE levels (factor 1.2-1.3) was observed after 6 h incubation. After 24 h incubation, the ADHE signal appeared fuzzy in strain CC-124 while it remained rather stable in strain 10-6C (Fig. 7B). We also followed PFL and PFO, the two enzymes which under anoxia can potentially produce acetyl-CoA, the substrate of ADHE (Fig. 1). During the first hours of dark incubation (up to 6 hours), no variation in the PFL levels were noticed. After 24 h, the PFL abundance was unchanged in the mutant strain while the protein could no longer be detected in the wild-type strain. For PFO, the antibodies failed to detect the protein levels under both oxic and anoxic conditions (not shown), in agreement with earlier studies (18) [van Lis et al., 2013). The RBCL abundance appeared stable over the incubation period in the mutant strain; in contrast, in the wild-type strain RBCL was no longer detected after 24 h incubation (Fig. 7B). Notably, the levels of subunit beta of the mitochondrial ATPase (ATP2) in both strains were stable over the whole period of dark anoxia (Fig. 7B). The increased abundance of subunit gamma of chloroplast ATPase (ATPC) observed in WT strain may be due to a relative overrepresentation of stable proteins when the total number and amount of proteins is dwindling. Of note, neither the overall protein profiles nor the ADHE abundance were affected by the HP-treatment (Supplemental Fig. S4). Thus, rather than inducing a protein remodeling in WT strain, it seems that prolonged dark anoxia has a deleterious effect on its overall proteome, likely representing a degradation of cell integrity. In contrast, the proteome of strain 10-6C, which exhibits higher ADHE levels, appears quite stable despite the prolonged anoxia. Strain 10-6C has been poorly characterized so far and the lack of knowledge on its genetic background hampered drawing firm conclusions as to the regulation of ADHE levels during aerobic growth and its role during fermentation.

Zinc-deficiency increases ADHE accumulation and fermentative abilities - In a study based on quantitative proteomics, it was reported that aerobic growth in conditions of zinc-deficiency increased the ADHE intracellular levels by 3-4 fold in strain CC-4532 (38). The increased ADHE abundance in zinc-deficient cells could be interpreted as a way to maintain a basal ADH capacity in the cell. Indeed, the replacement of the four predicted Zn-dependent ADHs (Cre09.g392134; Cre14.g623650; Cre03.g207800; Cre03.g207550) by functional homologs which rely on other metals, Fe in particular, could ensure optimal (fermentative) metabolism. We first checked the response of our reference strain CC-124 to zinc-deficiency. The alga was inoculated in TAP medium without $ZnSO_4$ and later transferred twice into this medium to reduce the intracellular zinc content. An increased abundance of chaperone Zcp2 (Supplemental Fig. S5) indicated the establishment of metal-deficiency (38) [Hsieh et al., 2012). Zinc-deficient CC-124 cells were found to contain ~3 times more ADHE than zinc-replete cells (Supplemental Fig. S5; Table 4), thus making them of value for our fermentation studies.

The response of zinc-deficient CC-124 cells to 24 h of dark anoxia was examined through the analysis of proteins and fermentation products (Fig. 8). HPLC analysis of excreted metabolites indicated the presence of formate, acetate and ethanol in a molar ratio of 2:1:1, being thus comparable to the ratio obtained with cells grown on standard TAP medium. The respective amounts of these products were however found to be two-fold higher in zinc-deficient cells as compared to zinc-replete cells (Fig. 8A), revealing the higher fermentative capacities of the metal-deficient cells. In contrast to zinc-replete CC-124 cells, the overall protein profile of zinc-deficient cells hardly changed after prolonged anoxia, as observed in strain 10-6C (Fig. 8B). Notably, the levels of ADHE, PFL, and the PTAs which compete with ADHE for acetyl-CoA (Fig. 1), appeared roughly unaffected by anoxia changed in zinc-deficient cells (Fig. 8C; Supplemental Fig. S6, S7). On the whole, these data had several implications: *i*) strain CC-124 is not intrinsically unfit to withstand prolonged anoxia; *ii*) zinc-deficiency enhances the cell capacity to survive anoxia and *iii*) in *Chlamydomonas*, the PFL-gated pathway appears as the preferred fermentative route irrespective of the cell's zinc status.

Evaluating ADHE accumulation in relation to starch levels - In the conditions of fermentation applied here, *i.e.* dark incubation in a potassium phosphate medium, starch content is believed to be key for the maintenance of cell integrity and survival. Indeed, starch is the source of glucose, directly fuelling glycolysis to produce ATP under anoxia (Fig. 1). We therefore examined the starch content in the cells analysed above. As shown in Fig. 9A, the amounts of starch in strain CC-124 increased 3-4 fold when zinc was removed from medium, reaching up to 5-6 µG starch per 10^6 cells. The analysis of cell sections by electron microscopy confirmed the higher starch content in zinc-deficient cells relative to zinc-replete cells (Fig. 9B). Of note, starch content in TAP-grown 10-6C cells was also higher than in the reference CC-124 cells, with *ca* 6-7 µG per 10^6 cells (not shown). These data thus suggest that the higher fermentation capacity of strain 10-6C and zinc-deficient CC-124 cells, relative to standard CC124 cells, is a direct result of a higher content in C-reserves. The associated increase in ADHE levels may be then projected to facilitate the ethanol fermentation of starch over longer periods.

To further evaluate the link between ADHE upregulation and starch accumulation, the protein abundance was followed after transferring the cells to TAP medium without ammonium (N-free medium). Such a medium is known to trigger the accumulation of large amounts of starch in the green alga *Chlamydomonas* (39). Time course experiments with long term sampling (0, 17 h, 24 h, 40 h, 49 h and 72 h) were carried out with strain CC-124. In our conditions, cellular starch content increased steadily during the first 2 days after transfer to N-free medium (Fig. 10). Followed by protein blots, the ADHE steady-state levels were found to increase progressively during the first 24 h (~2.5-fold), thus correlating with the increase in starch content (Fig. 10; Table 4). Later a slow decrease in the protein abundance was observed (Fig. 10). PFL levels appeared rather stable throughout the whole period, though a slight decrease was observed in the first hours of N-deprivation (Fig. 10). The behaviour of ADHE and PFL in response to N-starvation is interesting as it contrasts with that of a great number of chloroplast proteins, including enzymes of the Calvin cycle and components of the photosynthetic chain, whose levels decreased shortly after the transfer to N-free medium (40, 41). Here we observed within the first 24h of N-starvation, an important decrease (more than 50%) in the abundance of RBCL and phosphoribulokinase (PRK), two key enzymes of the CBB cycle, and of ADP-glucose pyrophosphorylase (AGPase; EC 2.7.7.27), the chloroplast enzyme that catalyzes the first committed step in starch synthesis. The decrease in AGPase is puzzling considering that starch content increases significantly during that same period (Fig. 11). ADHE thus occupies a position of priority amongst chloroplast proteins in conditions where N is limiting.

Finally, we wondered whether ADHE accumulation was linked to starch synthesis. For that, we used mutant strain Sta6, which is unable to synthesize starch because it lacks the AGPase small subunit (42). In this strain growing on standard TAP medium, ADHE is present at low levels, comparable to those in wild-type strain CC-124 (Table 4). The transfer of Sta6 cells to zinc-deficient TAP medium led to a ~3-fold increase in ADHE abundance (Table 4), similar to that observed with wild-type strain CC-124. From the study of starch-less strain sta6, it can be inferred that ADHE accumulation is not directly controlled by starch synthesis.

Evaluating ADHE accumulation in relation to CO_2 requirements - A well-documented effect of zinc-deficiency in *Chlamydomonas* is the impairment of carbon-concentrating mechanism (CCM) under atmospheric conditions (38, 43). We thus considered the possibility that the abovementioned rise in ADHE levels in zinc-deprived strains CC-124 and Sta6 might be a consequence of reduced CO_2 availability.

All the experiments described in this work were carried out with cells grown on TAP-derived media under atmospheric conditions (0.04% CO_2) at a light intensity of 40 µmol photons m^{-2} s^{-1}. In these conditions, the cells rely on CCM to concentrate CO_2 at the active site of the RubisCO (44). The ADHE abundance was evaluated in two mutant strains impaired in CCM: strain CIA5 lacks Ccm1, a master gene regulator that controls the induction of CCM by sensing CO_2 availability in *Chlamydomonas* (45, 46), and strain CIA3 which lacks CAH3, the thylakoid

lumen carbonic anhydrase which provides CO_2 to the RubisCO (47). The ADHE abundance in these two strains grown under atmospheric conditions was similar, and 1.5-1.8 fold higher than that in wild-type strain CC-124 (Table 4).

Additional observations provided further support for a link between the ADHE levels and the CO_2 availability: *i*) ADHE was hardly detected in wild-type strain CC-124 grown on TAP medium supplemented with 2% CO_2 (in these conditions CCM is not required) (Table 4); *ii*) ADHE was only faintly observed in strain ΔRBCL (Table 4), which lacks RubisCO due to a large deletion in the chloroplast RBCL gene (48). This strain, which is light-sensitive, relies mostly on mitochondrial metabolism for growth (49), 2014); and *iii*) in the 5' UTR of the ADHE gene a typical low CO_2 cis-acting enhancer element was identified (GAGTTGC; position -299 to -293 from the ATG) (50), which argues for the upregulation of the ADHE expression under low CO_2.

Light was also found to influence the ADHE abundance in *Chlamydomonas*. Wild-type CC-124 cells were grown to early log-phase on TAP medium at a light intensity of 40 µmol photons m^{-2} s^{-1} and later exposed to different light intensities for 20 h. Cells grown at 15 and 40 µmol photons $m^{-2}.s^{-1}$ exhibited similar amounts of ADHE while cells grown at 200 µmol photons $m^{-2}.s^{-1}$, contained slightly more ADHE (Table 4). At higher light intensity, the cells require more CO_2 which may not be fulfilled under the atmospheric conditions and thus constitute a signal for ADHE accumulation.

DISCUSSION

Bifunctional aldehyde/alcohol dehydrogenases are present in a variety of facultative and strict anaerobic bacteria, but remains so far undetected in Archaea. In the eukaryotic world, ADHEs have long been thought to be restricted to anaerobic species (pathogens). But over the last decade, ADHE genes have been uncovered in species of varied lifestyles. In particular, ADHEs have been found in photosynthetic microalgae thriving in fresh or marine waters (14). Despite the significant set of bacterial and eukaryotic ADHE sequences used in our phylogenetic analysis (Supplemental Data Set 1), the evolutionary history of eukaryote enzymes remains confusing. Only in the case of photosynthetic microalgae, the ADHE is found in two distinct positions in the tree (Fig. 2): the enzymes in *B. natans* and *G. theta*, are found among most of their counterparts in anaerobic eukaryotes between the two bacterial protein clusters, while the chlorophyte ADHEs are found in cluster I, in close proximity to the cyanobacterial counterparts (Fig. 2). Hence, at least two different ADHE gene donors have to be considered in the evolution of unicellular algae. For the chlorophytes, a vertical inheritance of ADHE from cyanobacteria appears sound, especially because the enzyme is present in the species of the orders Nostocales and Stigonematales, proposed to be at the origin of all primary plastids (51). Puzzling though is that ADHE genes have not been found in the sequenced genomes of *Cyanophora paradoxa* (a glaucophyte) and of *Porphyra* species (rhodophytes), which are believed to have emerged with the chlorophytes from the same unique cyanobacterial endosymbiosis (52). To determine whether these species represent special cases or whether the rhodophytes and glaucophytes have lost the ADHE gene prior to their radiations, it is essential to obtain more genome sequences from these algal lineages.

Chlamydomonas is the first eukaryote known so far in which the ADHE localizes to the chloroplast; such a compartmentalization is likely reminiscent of the cyanobacterial ancestor. In spite of the chloroplast confinement, the algal ADHE exhibits molecular and enzymatic traits comparable to those of its counterparts in bacteria and amitochondriate eukaryotes. This is significant because ADHE is known as a major target of metal-catalyzed oxidation (MCO) (53). In this process, Fe^{2+} ions in the protein active site (see Fig. 1) react with ROS and generate hydroxyl radicals. In turn, these radicals can selectively oxidize the nearby His residue, leading to the irreversible inactivation of the enzyme. Also interesting is the fact that the ADHE assembly in long filaments can also take place in the oxygen-rich atmosphere of the chloroplast.

Previous studies on the fermentative capacities of *Chlamydomonas* indicated that both the chloroplast and the mitochondria contained a complete PFL-gated pathway, composed of a PFL, a PTA-ACK and an ADHE (8). While the presence of a PFL and

PTA-ACK in mitochondria has been confirmed by biochemical and molecular approaches (12, 24), the attempts to detect an ADHE have failed as yet (12, 33) (Fig. 4). Further studies will determine whether PFL and PTA-ACK form a pathway leading to formate and acetate or whether they act independently in the mitochondrion.

Our study adds further evidence to the notion that decreased oxygen availability is not a signal for ADHE accumulation in *Chlamydomonas* (Fig. 6). In this respect, the microalga differs from the facultative anaerobic bacteria studied to date. In *E. coli*, for example, ADHE abundance increases up to 10-fold upon exposure to anoxia (54). In *S. aureus*, ADHE is a target of the redox sensing transcriptional regulator Rex, which regulates most genes encoding fermentative enzymes (55). The few data on photosynthetic bacteria (cyanobacteria) also point at a regulation by anoxia: the AdhE transcripts in *Synechococcus* species in microbial mats (Octopus Spring, Yellowstone National Park) were shown to increase during the evening (56). The rationale for the different enzyme regulation between facultative anaerobic bacteria and *Chlamydomonas* is likely to be found in differences in lifestyle and cell complexity. The constitutive accumulation in the alga might specify the need to respond quickly to dark anoxia. It could make good sense for *Chlamydomonas* to produce ADHE, a large protein, during aerobic conditions when energy is not usually limiting rather than under anoxia, when ATP is in short supply. This also holds for PFL, which accumulates under aerobic conditions (12) (Figs. 7, 8). Alternatively, the accumulation of ADHE under oxic conditions could indicate that the enzyme is also required in aerated environments. Production of ethanol under atmospheric conditions, as it happens in *S. cerevisiae*, seems unlikely as ethanol has not been detected in the culture medium of aerobically growing algae (not shown). The ADHE in the alga could also have a function not directly linked to ethanol metabolism, as reported recently in *E. coli* (57, 58).

Throughout this work we have identified a few mutant strains and physiological conditions that influence the ADHE levels in the microalga. Increased ADHE abundance was observed in cells growing on TAP medium lacking zinc or a nitrogen source (Figs 8 and 10), in mutant strains impaired in the carbon concentrating mechanism (CIA5 and CIA3), in cells lacking RubisCO carboxylase activity (strain 10-6C) or even in conditions of high light (Table 4). Inversely, ADHE was hardly detected in cells which do not rely on CCM for growth (Table 4). A possible rationale for an increased ADHE abundance in conditions where carbon-concentration is impaired may relate to an over-reduction state of the chloroplast: low CO_2 or the absence of CBB cycle activity will strongly lower CO_2 reduction, which is a major electron sink in the light. Our data showed that in several cases, high ADHE levels coincide with high starch content in the cell. Interestingly, our data showed that enhanced ADHE levels coincide with higher starch content in the cells; that is the case of cells growing on TAP medium lacking zinc or a nitrogen source and in cells lacking RubisCO carboxylase activity (strain 10-6C) (Fig. 8 and 10). As said early, we identified a cis-acting element in the promotor region of the ADHE gene which could provide a rationale for the observed regulatory influence of CO_2. Importantly, the same type of element was found in the AGPase, the rate-limiting enzyme involved in starch synthesis. A concerted induction by low CO_2 could constitute a direct link between ADHE and starch synthesis. The concerted accumulation of ADHE and starch may also result from an increase in ATP and NADPH levels in response to a lower RubisCO activity.

In our experimental conditions, the alga ferments its carbon stores mainly into formate, acetate and ethanol in a molar ratio of 2:1:1. This mixed-acid fermentation indicates the involvement of a metabolic pathway gated through PFL. The use of this route has a clear advantage over other more typical routes in eukaryotes (PDC/ADH or LDH) (Fig. 1) as it balances NAD+ regeneration with the need for energy production in conditions of dark anoxia. Here we showed that cells with elevated ADHE levels (strain 10-6C and zinc-deprived strain CC-124) exhibit the same mixed-acid fermentation but have extended fermentation abilities. From the product yields at 24 h (Fig. 6, 7), it is inferred that the fermentation span extends up to 16 h. Furthermore, our results revealed the higher stability of the overall proteome in cells with

enhanced ADHE levels. After 24 h of dark anoxia, the protein profiles of the cells with higher ADHE content were shown to be unaltered, contrasting with the situation in reference cells where protein degradation, in particular degradation of fermentative enzymes, occurs. Cells with higher ADHE thus appear to be better suited to survive under dark anoxia, which appears most immediately linked to the content in endogenous carbohydrate content. If we assume that ADHE is only required for anaerobic metabolism, it could be hypothesized that the high ADHE content, that seems intricately linked to high starch levels, anticipates the loss of protein due to inactivation and/or degradation that inevitably occurs over the extended fermentation periods that higher starch stores will allow. The question if an increased ADHE level is indeed crucial for anoxic survival remains to be answered since we have not identified a condition or strain where high starch coincides with low amounts of ADHE. The amazing ability of *Chlamydomonas* to survive over long period under dark anoxia was in some way unexpected for a photosynthetic alga that typically lives in mid latitudes where day (light) length varies only moderately. It would thus appear that other conditions than light also determine to what extent the algal cell is in fact exposed to conditions of dark anoxia.

We believe that the present study forms a solid basis for further studies to identify the molecular basis of the ADHE regulation in *Chlamydomonas*. The predominant role of ADHE in the fermentation metabolism of the green alga is confirmed here but our studies cannot rule out the possibility that this enzyme has other functions (under oxic conditions). To elucidate the mechanism underlying the aldehyde/alcohol dehydrogenase upregulation as well as to identify potential alternative functions for ADHE in the green alga, the examination of the counterpart from diverse biochemical context and thriving in different environments is expected to provide valuable insights. Among the ADHEs that would deserve scrutiny are those from cyanobacteria, and from non-chlorophyte photosynthetic algae, such as the members of the SAR supergroup, in which the repertoire of fermentative enzymes is distinct from that in chlorophytes (14).

EXPERIMENTAL PROCEDURES

Chlamydomonas strains, media and culture conditions- From the *Chlamydomonas* Resource Center (http://chlamycollection.org/; Minnesota University) the following strains were obtained: CC-124 (137c mt- nit1- nit 2-), CC-4348 (sta6-1 mt+), and CC-2702 (CIA5). From the ChlamyStation Collection (http://chlamystation.free.fr/) (CNRS UMR7141, Paris) were obtained the RubisCO mutants 10-6C.arg2.mt+ and ΔRbcL 1.7.5. The presence of the point mutation Gly-171-Asp in RBCL which confers impaired CO_2 fixation in strain 10-6C (31-32) was confirmed in this work by protein-based mass spectrometry analysis (Supplemental Figure S2). Strain CIA3 was a gift from Göran Samuelsson (Umeå University, Sweden). All strains were maintained at 24°C on Tris-Acetate-Phosphate (TAP) medium (59) containing 1.5 % agar. For strain 10-6C.arg2.mt+, TAP medium was supplemented with arginine (100 mg/mL). All media were prepared with MilliQ water.

The cells were grown in flasks on Tris-Acetate-Phosphate (TAP) medium unless otherwise stated. Flasks were placed in an Innova incubator (NewBrunswick Scientific) at 125 rpm under continuous light, at 24°C. Cells were routinely grown at a light intensity of 40-50 µmol photons m^{-2} s^{-1}, except strain ΔRbcL 1.7.5 at 10-15 µmol photons m^{-2} s^{-1}. Wild-type strain CC-124 was also grown at 15 and 200 µmol photons m^{-2} s^{-1}. For growth in absence of zinc, the culture medium was prepared by omitting $ZnSO_4$ from the standard TAP medium. Cells from TAP plates were inoculated into 100-mL of "zinc-free" medium and grown to their late log-phase. Cells were then transferred into a fresh medium without zinc at a cell concentration of ~ 1 x 10^5 cells mL^{-1}. Zinc-deficiency was reached after a third round of transfer into "zinc-free" medium. The analyses of zinc-deficient cells were carried out on cells harvested in their mid-log phase. N-free medium was prepared by omitting ammonium chloride from the TAP medium. Cells subjected to N-deprivation were grown to 3-4 x 10^6 cells mL^{-1} and collected by centrifugation at 1,500*g* for 5 min at room temperature. Cells were washed in N-free TAP medium and finally resuspended in N-free TAP to ~1 x 10^6 cells mL^{-1}. For experiments involving CO_2 supplementation, cultures were grown in an incubator bubbled with an atmosphere of 2% CO_2 in air. Cell densities were determined using a Malassez hemocytometer after addition of Lugol (Sigma-Aldrich) to the cell suspension to immobilize the cells.

Organelle isolation, and partial purification of chloroplast ADHE- Isolation of chloroplasts and mitochondria from mutant strain 10-6C was essentially as described in (60). For the ADHE partial purification, the chloroplasts were resuspended in Hepes 50mM, pH 7.0 in presence of protease inhibitors (0.5 mM benzamidine and 1 mM aminocaproïc acid) to a final protein concentration of 5 mG/mL, frozen and thawed twice and centrifuged at 11,000 *g* for 15 min at 4°C. The ADHE-containing supernatant was applied to an anion exchange Ceramic HyperD® resin (GE Healthcare), equilibrated and eluted with Hepes 50mM, pH 7.0. In these conditions, ADHE was not retained on the column. ADHE in the flow-through was either pelleted by ultracentrifugation at 110,000 *g* for 1 hour (4°C) or applied on a Blue Sepharose 6 (GE Healthcare). Elution from the Blue resin was achieved with 1 M NaCl in Hepes 50mM, pH 7.0.

Mass spectrometry analysis- For mass spectrometry analysis, different samples were analyzed. Whole chloroplasts were loaded on 6M urea/SDS-PAGE (5-12% acrylamide) and gel bands containing PTAs (80 kDa), RBCL (45 kDa) and ADHE (100-kDa) were cut out. ADHE was also identified in whole cell lysate and in a chloroplast soluble fraction. For the 2 latter samples, 3-4 µg of proteins were stacked at the top of a 10% acrylamide gel and gel bands containing the concentrated proteins were cut out. All gel bands were cut in pieces before being washed by 6 successive incubations of 15 min in 25 mM NH_4HCO_3 and in 25mM NH_4HCO_3 containing 50% (v/v) acetonitrile. Gel pieces were then dehydrated with 100 % acetonitrile and incubated for 45 min at 53°C with 10 mM DTT in 25mM NH_4HCO_3 and for 35 min in the dark with 55 mM iodoacetamide in 25mM NH_4HCO_3. Alkylation was stopped by adding 10 mM DTT in 25mM NH_4HCO_3 and mixing for 10 min. Gel pieces were then washed again by incubation in 25 mM NH_4HCO_3 before dehydration with 100% acetonitrile. Modified trypsin (Promega, sequencing grade) in 25 mM NH_4HCO_3 was added to the dehydrated gel pieces for an overnight incubation at 37°C. Peptides were then extracted in three sequential extraction steps (15 min each) in 30 µL of 50% acetonitrile, 30 µL of 5% formic acid and finally 30µL of 100% acetonitrile. The pooled supernatants were then dried under vacuum.

The dried extracted peptides were resuspended in 5% acetonitrile and 0.1% trifluoroacetic acid and analyzed by online nanoLC-MS/MS (Ultimate 3000, Dionex and LTQ-Orbitrap Velos pro, Thermo Scientific). Peptides were sampled on a 300 µm x 5 mm PepMap C18 precolumn and separated on a 75 µm x 250 mm C18 column (PepMap, Dionex). The nanoLC methods consisted in 25 and 120-minutes acetronitrile gradients in 0.1% formic acid at a flow rate of 300 nL/min for, respectively gel band and stacking analyses. MS and MS/MS (Top20) data were acquired using Xcalibur (Thermo Scientific) and processed automatically using Mascot Daemon software (version 2.5, Matrix Science). Searches against the Phytozome database (v9.0, *Chlamydomonas reinhardtii* taxonomy) (61), a home-made classical contaminants database and the corresponding reversed databases were performed using Mascot (version 2.5.1). ESI-TRAP was chosen as the instrument, trypsin/P as the enzyme and 2 missed cleavages allowed. Precursor and fragment mass error tolerances were set respectively at 10 ppm and 0.6 Da. Peptide modifications allowed during the search were: carbamidomethyl (C, fixed) acetyl (N-ter, variable) and oxidation (M, variable). The IRMa software (62) (version 1.31.1) was used to filter the results: conservation of rank 1 peptides, peptide identification FDR < 1% (as calculated on peptide scores by employing the reverse database strategy), and minimum of 1 specific peptide per identified protein group.

Dark fermentation- Five hundred-to- 700 mL of cultures in their mid-log phase were harvested, washed in 10 mL of filtered-sterilized anaerobic induction buffer (AIB) medium, and finally resuspended in AIB medium to a cell concentration of *ca* 1 x 10^7 cells mL^{-1}. Thirty mL of cell suspension was transferred to a 60-mL glass serum bottle. Bottles were closed with a butyl rubber stopper, wrapped in aluminium foil, degassed for 10 min, and then purged with argon for 15 min. Bottles were placed in an incubator at 24°C and agitated at 125 rpm. Where indicated, sodium hypophosphite (at a final concentration of 10 mM) was added to the cell suspension. Anaerobic samples were taken regularly and processed for the analysis of protein, fermentation products and starch content (see below). After each sampling, the bottles were flushed with argon.

Analysis of fermentation products- Cells acclimated to dark anoxia were harvested by centrifugation (7 min at 14,000 x g). The resulting supernatants were filtered through a nylon filter (0.2 µm) and frozen until use. Prior to the analysis by high pressure liquid chromatography (HPLC) (Agilent 1260), the samples were diluted twice in 10 mM H_2SO_4 and centrifuged briefly. The fermentative products were then separated using a HiPlex-H column for carbohydrates, organic acids and alcohols (300 x 7.7 mm, 8 µm; Agilent) at 50°C; the mobile phase was 10 mM sulfuric acid and the flow rate 0.6 mL/min. Detection was done with a refractive index detector (50°C) and a photodiode array detector operating at 210 and 280 nm. The predominant products were identified as formate (14 min), acetate (15.3 min) and ethanol (21.7 min). Signals were integrated and metabolites quantified using a standard curve generated for each metabolite detected.

Starch quantification -Cells (2-5 x 10^6 cells) from cultures or anaerobic incubations were collected by centrifugation (5 min at 14,000*g*) and frozen in liquid nitrogen until use. To disrupt cell integrity and extract pigments, 1 mL of 80% acetone is added to each cell pellet. The cell residues obtained after centrifugation were rinsed with 0.5 mL of 100 mM Na-acetate buffer (pH 4.5), then resuspended in 300 µL of the same buffer, heat-treated 20 min at 120°C for starch solubilization. Total starch was quantified using an enzymatic starch assay kit including amyloglucosidase, hexokinase and glucose-6-phosphate dehydrogenase (R-Biopharm, Darmstadt). Alternatively, solubilized starch was stained using a commercial iodine solution (Sigma) as follows: 100 µL of solubilized starch were mixed to 800 µL of water and 100 µL of Lugol. Absorbance was measured spectrophotometrically at 580 nm. Quantification was done using commercial starch (R-Biopharm). Results from both methods were comparable.

Determination of protein concentration, SDS-PAGE and immunodetection- Protein concentrations were routinely determined using the bicinchoninic acid (BCA) based Thermo Pierce® Protein assay kit, using bovine serum albumin as standard. When protein concentrations of cell extracts were to be determined, proteins were first precipitated by $CHCl_3$/MeOH (63) and then resuspended in 2% SDS (w/v). Proteins were analyzed either on 10% acrylamide SDS-PAGE, 7.5-

12% acrylamide SDS-PAGE or 5-12% acrylamide gels containing 6M urea (urea/SDS-PAGE). Protein samples (40 µG) were resuspended in 2% SDS (w/v) and 2% beta-mercaptoethanol, and boiled for 90 sec. Insoluble material was then removed via a 2 min-centrifugation at 13,000*g*. Apparent molecular masses were estimated using Prestained protein ladder Plus (Euromedex). After electrophoresis, proteins were either stained with Coomassie Blue R250 or with Ponceau S after transfer onto nitrocellulose membranes.

Immunoblotting experiments were carried out following a standard protocol at room temperature. Nitrocellulose membranes were first blocked for one hour in 20 mM Tris, 300 mM NaCl, pH 7.5 supplemented with 0.1% Tween-20 (T-TBS) before incubation with primary antibodies for 1 hr. The primary antibodies were from various sources. From Agrisera AB (Vännäs, Sweden) were purchased antibodies against ADGP (AS11 1739), ATPC (AS08 312), CAH3 (AS05073), HydA (AS09514), PDC (AS10691), and RbcL (AS03037). Antibodies against ADHE, PFL and ATP2 were described in (Atteia et al., 2006). Antibodies to PTAs were generated by immunization using heterologous protein (see Supplemental Figures S6 and S7). Anti-LHC was from O. Vallon (IBPC, Paris) and anti-PRK from Mike Salvucci (USDA, Washington D.C.). The Zcp2 antibodies were a gift from S. Merchant (U.C.L.A). Anti-rabbit IgG peroxidase conjugate (Sigma-Aldrich) was used as secondary antibody. Immunochemical detection was carried out using the homemade enhanced chemiluminescence system (64) and Image Quant LAS 4000 mini (GE).

BN-PAGE and two-dimensional SDS-PAGE- BN-PAGE was carried out using a 3-12% linear polyacrylamide gradient (Atteia et al., 2003). Freshly purified rADHE (25 µG) was supplemented with loading buffer that contains 30 mG/mL Blue G in Tricine 50 mM, pH 8.0. Electrophoresis was carried out at 4°C at constant current (10 mA) for ~1h. The molecular mass of the rADHE oligomers separated on BN-PAGE were evaluated using commercial molecular mass markers (bovine serum albumin (66 kDa), *S. cerevisiae* alcohol dehydrogenase (150 kDa), horse spleen apoferritin (443 kDa) and bovine thyroglobulin (669 kDa) (Sigma-Aldrich). In-gel alcohol dehydrogenase activity assay was performed at room temperature as follows. A BN-gel lane was washed twice in 100 mM Tris, pH 8.8 and then incubated in 25 mL of 100 mM Tris-Cl pH 8.8 containing 20 mg of NAD, 5 mg of nitroblue tetrazolium (NBT), 1 mg of phenazine methosulfate (PMS) and 25 µL of absolute ethanol. In the presence of PMS, NBT reacts with NADH produced by dehydrogenases to produce an insoluble blue-purple formazan precipitate. For two-dimensional (2D)-BN/SDS-PAGE, a BN-gel lane was cut out after the run, washed three times 5 min in 1% SDS and 1% 2-mercaptoethanol, and then applied on top of a 10% SDS-PAGE gel. After electrophoresis, proteins were transferred onto nitrocellulose membrane.

Expression and purification of Chlamydomonas ADHE- The coding region of *C. reinhardtii* ADHE was amplified using the following pair of primers: CrADHE_NdeI gaccatatgGCCGCTGCCCCGGCCACCC (61-AAAPAT-66) and CrADHE_XhoI gtcctcgagGTTGATCTTGGAGAAGAACTC (948-EFFSKIN-954) using as template the full-length cDNA (CAF04128). The amplified fragment was cloned into the pET-24a expression vector (Novagen) using the XhoI and NdeI restriction sites within the multiple cloning site to incorporate a C-terminal 6 His tag. The sequence of the clone pET24a-CrADHE was confirmed at GATC Biotech. *E. coli* BL21 (DE3) cells were transformed with this construct. Transformed cells from plates were inoculated in the auto-induction medium ZYM2052 (65) and grown overnight at 37°C. The cells were harvested, washed once in Buffer 1 (300 mM NaCl, 50 mM sodium phosphate, pH 8.0) and frozen. Purification of ADHE was performed the same day at 4°C under argon. Cells were resuspended in Buffer 1 supplemented with 0.5 mg/ml lysozyme, 0.5 mg/mL DNase and 2 mM $MgCl_2$ and protease inhibitors (PMSF, amino caproic acid, benzamidine) and then broken by three cycles of freezing (liquid nitrogen) and thawing. The broken cells were centrifuged at 10,000 x *g* for 15 min, at 4°C. The supernatant was collected and gently mixed with HIS-Select Nickel Affinity gel (Sigma-Aldrich). The mixture was then poured into an empty column. The gel was extensively washed with 10 mM imidazole in Buffer 1. The His-tagged ADHE was eluted with 100 mM imidazole in Buffer 1, quickly desalted on a PD10 column pre-equilibrated with 50 mM Tricine, pH 8.0, and finally concentrated on a Vivaspin 30 (cut off 30 kDa) (GE Healthcare) to reach a final concentration of 5-7 mg protein/mL

Enzyme assays- Freshly prepared ADHE was tested for the different enzymatic activities, at 25°C. Standard assay medium for NADH-dependent reactions consisted of 50 mM potassium phosphate pH 7.0 and 0.4 2 mM NADH. Acetyl-CoA reductase activity was determined in the presence of 0.21 mM acetyl-CoA; acetaldehyde reductase was determined with 1 mM acetaldehyde and 0.21 mM CoASH. The rate of both reductase reactions were monitored spectrophotometrically following the disappearance of NADH at 340 nm. Standard assay medium for NAD^+ -dependent reactions contained 1.5 mM NAD^+ in 50 mM Glycine/NaOH buffer pH 9.0. Ethanol dehydrogenase activity was assayed in 170 mM ethanol (1% v/v);; acetaldehyde dehydrogenase activity was assayed in 1 mM acetaldehyde and 0.2 mM CoASH. The rates of both dehydrogenases were monitored by the formation of NADH at 340 nm. All reactions were started by the addition of 25-40 µg purified enzyme. In all the assays, one unit of enzyme activity (U) was defined as 1 µmol of NADH converted per min.

Electron microscopy- Negative staining: 5 µl drops of the protein suspension were placed directly on glow discharged carbon coated grids (EMS) for 3 min. The grids were then washed with two drops of 2% uranyl acetate in water, and stained with a third drop for 1 min. Grids were dried on filter paper and the samples were analyzed using a Tecnai 200KV (operated at 120KV) electron microscope (FEI). Digital acquisitions were made with a numeric camera (Eagle, FEI). Morphology: In preparation for high-pressure freezing, aliquots of the liquid cultures are transferred to 50 ml conical centrifuge tubes, spun at 500 *g* for 5 min, and then gently resuspended in the growth medium containing 150 mM mannitol (66). Subsequently the cells were pelleted, high pressure frozen, freeze substituted, embedded in LR White resin (Hard Grade), according to McDonald (2014). Ultrathin cryosections were prepared with an ultracryomicrotome (EM UC7 Leica).

Bioinformatic and Phylogenetic Analyses- Sequence alignments were done with the Muscle module as part of the MEGA 6 program (Tamura et al., 2013) (http://megasoftware.net/mega.php) and manually adjusted to optimize alignments. The maximum likelihood phylogenetic tree was also produced using the MEGA 6 program. Conserved domains in *Cr*ADHE were identified using the NCBI-CDD database (http://www.ncbi.nlm.nih.gov/Structure/cdd/cdd.shtml). Iron-binding signatures were identified using the database of protein domains, families and functional sites Prosite (http://prosite.expasy.org/). Intracellular targeting prediction was carried out using the multi-subcellular localization prediction tool Predalgo, dedicated to green algae (https://giavap-genomes.ibpc.fr/cgi-bin/predalgodb.perl?page=main) (Tardif et al., 2012). Protein quantification was done on Western-blots using ImageJ (http://rsb.info.nih.gov/ij/index.html).

Conflicts of interest: The authors declare they have no conflicts of interest with the contents of this article.

Author contribution

A.A., R.vL, D.D. designed the research. A.A., R.vL., M.P. performed research. R.vL. and W.N. phylogenetic analyses; Y.C. carried out the proteomic analyses. A.K. performed electron microscopy. A.A. and R.vL wrote the article with contributions of all the authors.

Acknowledgements

This work was supported by the Centre National de la Recherche Scientifique and partly supported by the Agence Nationale pour la Recherche (ANR-11-BIOE-004-03) (A.A., R.vL, M.P.) the ProFi Infrastructure grant (ANR-10-INBS-08-01) (Y.C.). Thanks are due to Dr. Göran Samuelsson (Umeå University, Sweden) for providing strain cia3; to Dr. Joanna Porankiewicz-Asplund (Agrisera) for several useful insights regarding the antibodies; to Sabeeha Merchant (U.C.L.A) for the antibodies to ZCP2 and discussions on zinc-deficiency at the early stage of this work; to Sandrine Bujaldon (IBPC) for various discussions around the strains and for fluorescence measurements; and to Jean-François Sassi (Cité des Energies, CEA-Cadarache) for the cultures in 2% CO_2.

References

1. Oren, A., and Shilo, M. (1979) Anaerobic heterotrophic dark metabolism in the cyanobacterium *Oscillatoria limnetica*: sulfur respiration and lactate fermentation. *Arch. Microbiol*. **122**, 77-84
2. Moezelaar, R., Bijvank, S.M., and Stal, L.J. (1996) Fermentation and Sulfur Reduction in the Mat-Building Cyanobacterium Microcoleus chthonoplastes. *Appl. Environ. Microbiol.* **62**, 1752-1758
3. Hoffmeister, M., van der Klei, A., Rotte, C., van Grinsven, K.W., van Hellemond,,J.J., Henze, K., Tielens, A.G., and Martin, W. (2004) *Euglena gracilis* rhodoquinone:ubiquinone ratio and mitochondrial proteome differ under aerobic and anaerobic conditions. *J. Biol. Chem.* **279**, 22422-22429
4. Müller, M., Mentel, M., van Hellemond, J.J., Henze, K., Woehle, C., Gould, S.B., Yu, R.Y., van der Giezen, M., Tielens, A.G., and Martin, W.F. (2012) Biochemistry and evolution of anaerobic energy metabolism in eukaryotes. *Microbiol. Mol. Biol. Rev.* **76**, 444-495
5. Stal L. J. and Moezelaar R. (1997) Fermentation in cyanobacteria. *FEMS Microbiol Rev.* **21**, 179–211
6. Kreuzberg, K. (1984) Starch fermentation via a formate producing pathway in *Chlamydomonas reinhardtii*, *Chlorogonium elongatum* and *Chlorella fusca*. *Physiol. Plant.* **61**, 87-94
7. Gfeller, R.P., and Gibbs, M. (1984) Fermentative Metabolism of *Chlamydomonas reinhardtii*: I. Analysis of Fermentative Products from Starch in Dark and Light. *Plant Physiol*. **75**, 212-218
8. Kreuzberg, K., Klock, G., and Grobheiser, D. (1987) Subcellular distribution of pyruvate-degrading enzymes in *Chlamydomonas reinhardtii* studied by an improved protoplast fractionation procedure. *Physiol Plantarum*. **69**, 481-488
9. Maione, T.E., and Gibbs, M. (1986) Hydrogenase-Mediated Activities in Isolated Chloroplasts of *Chlamydomonas reinhardii*. *Plant Physiol*. **80**, 360-363
10. Merchant, S.S., et al. (2007) The *Chlamydomonas* genome reveals the evolution of key animal and plant functions. *Science*. **318**, 245-250
11. Blanc, G., Duncan, G., Agarkova, I., Borodovsky, M., Gurnon, J., Kuo, A., Lindquist, E., Lucas, S., Pangilinan, J., Polle, J., Salamov, A., Terry, A., Yamada, T., Dunigan, D.D., Grigoriev, I.V., Claverie, J.M., and Van Etten, J.L. (2010) The *Chlorella variabilis* NC64A genome reveals adaptation to photosymbiosis, coevolution with viruses, and cryptic sex. *Plant Cell.* **22**, 2943-2955
12. Atteia, A., van Lis, R., Gelius-Dietrich, G., Adrait, A., Garin, J., Joyard, J., Rolland, N., and Martin, W. (2006) Pyruvate formate-lyase and a novel route of eukaryotic ATP-synthesis in *Chlamydomonas* mitochondria. *J Biol Chem.* **281**, 9909-991
13. Mus, F., Dubini, A., Seibert, M., Posewitz, M.C. and Grossman, A.R. (2007) Anaerobic acclimation in *Chlamydomonas reinhardtii*: anoxic gene expression, hydrogenase induction, and metabolic pathways. *J Biol Chem.* **282**, 25475-25486
14. Atteia, A., van Lis, R., Tielens, A.G.M., and Martin, W. (2013) Anaerobic energy metabolism in unicellular photosynthetic eukaryotes. *Biochem Biophys Acta* **1827**, 210-223
15. Happe, T., and Naber, J.D. (1993) Isolation, characterization and N-terminal amino acid sequence of hydrogenase from the green alga *Chlamydomonas reinhardtii*. *Eur J Biochem*. **214**, 475-481
16. Hemschemeier, A., Jacobs, J., and Happe, T. (2008) Biochemical and physiological characterization of the pyruvate formate-lyase Pfl1 of *Chlamydomonas reinhardtii*, a typically bacterial enzyme in a eukaryotic alga. *Eukaryot Cell.* **7**, 518-526
17. Silakov, A., Kamp, C., Reijerse, E., Happe, T., and Lubitz, W. (2009) Spectroelectrochemical characterization of the active site of the [FeFe] hydrogenase HydA1 from *Chlamydomonas reinhardtii*. *Biochemistry*. **48**, 7780-7786
18. van Lis, R., Baffert, C., Couté, Y., Nitschke, W., and Atteia, A. (2013) *Chlamydomonas reinhardtii* chloroplasts contain a homodimeric pyruvate:ferredoxin oxidoreductase that functions with FDX1. *Plant Physiol*. **161**, 57-71
19. Noth, J., Krawietz, D., Hemschemeier, A., and Happe, T. (2013) Pyruvate:ferredoxin oxidoreductase is coupled to light-independent hydrogen production in *Chlamydomonas reinhardtii*. *J Biol Chem*. **288**, 4368-4377
20. Dubini, A., Mus, F., Seibert, M., Grossman, A.R., and Posewitz, M.C. (2009) Flexibility in anaerobic metabolism as revealed in a mutant of *Chlamydomonas reinhardtii* lacking hydrogenase activity. *J. Biol. Chem*. **284**, 7201-7213

21. Philipps, G., Krawietz, D., Hemschemeier, A., and Happe, T. (2011) A pyruvate formate lyase-deficient *Chlamydomonas reinhardtii* strain provides evidence for a link between fermentation and hydrogen production in green algae. *Plant J*. **66**, 330-340
22. Magneschi, L., Catalanotti, C., Subramanian, V., Dubini, A., Yang, W., Mus, F., Posewitz, M.C., Seibert, M., Perata, P., and Grossman, A.R. (2012) A mutant in the ADH1 gene of *Chlamydomonas reinhardtii* elicits metabolic restructuring during anaerobiosis. *Plant Physiol.* **158**, 1293-1305
23. Catalanotti, C., Dubini, A., Subramanian, V., Yang, W., Magneschi, L., Mus, F., Seibert, M., Posewitz, M.C., and Grossman, A.R. (2012) Altered fermentative metabolism in *Chlamydomonas reinhardtii* mutants lacking pyruvate formate lyase and both pyruvate formate lyase and alcohol dehydrogenase. *Plant Cell*. **24**, 692-707
24. Yang, W., Catalanotti, C., D'Adamo, S., Wittkopp, T.M., Ingram-Smith, C.J., Mackinder, L., Miller, T.E., Heuberger, A.L., Peers, G., Smith, K.S., Jonikas, M.C., Grossman, A.R., and Posewitz M.C. (2014) Alternative acetate production pathways in *Chlamydomonas reinhardtii* during dark anoxia and the dominant role of chloroplasts in fermentative acetate production. *Plant Cell*. **26**, 4499-4518
25. Burgess, S.J., Taha, H., Yeoman, J.A., Iamshanova, O., Chan, K.X., Boehm, M., Behrends, V., Bundy, J.G., Bialek, W., Murray, J.W., and Nixon, P.J. (2016) Identification of the elusive pyruvate reductase of *Chlamydomonas reinhardtii* chloroplasts. *Plant Cell. Physiol*. **57**, 82-94
26. Adl, S.M., et al. (2012) The revised classification of eukaryotes. *J. Eukaryot. Microbiol*. **59**, 429-493
27. Atteia, A., van Lis, R., Mendoza-Hernández, G., Henze, K., Martin, W., Riveros-Rosas, H., and González-Halphen, D. (2003) Bifunctional aldehyde/alcohol dehydrogenase (ADHE) in chlorophyte algal mitochondria. *Plant Mol. Biol*. **53**, 175-188
28. Bruchhaus, I., and Tannich, E. (1994) Purification and molecular characterization of the NAD(+)-dependent acetaldehyde/alcohol dehydrogenase from *Entamoeba histolytica*. *Biochem J*. **303**, 743-748
29. Yang, W., Li, E., Kairong, T., and Stanley, S.L. Jr (1994) *Entamoeba histolytica* has an alcohol dehydrogenase homologous to the multifunctional adhE gene product of *Escherichia coli. Mol. Biochem. Parasitol.* **64**, 253-260
30. Sánchez, L.B. (1998) Aldehyde dehydrogenase (CoA-acetylating) and the mechanism of ethanol formation in the amitochondriate protist, *Giardia lamblia*. *Arch. Biochem. Biophys*. **354**, 57-64
31. Spreitzer, R.J., and Mets, L.J. (1980) Non-mendelian mutation affecting ribulose-1,5-biphosphate carboxylase structure and activity. *Nature*. **285**, 114-115
32. Dron, M., Rahire, M., Rochaix, J.D., and Mets, L. (1983) First DNA sequence of a chloroplast mutation: A missense alteration in the ribulose biphosphate carboxylase large subunit gene. *Plasmid*. **9**, 321-324
33. Terashima, M., Specht, M., Naumann, B., and Hippler M. (2010) Characterizing the anaerobic response of *Chlamydomonas reinhardtii* by quantitative proteomics. *Mol. Cell. Proteomics*. **9**, 1514-1532
34. Boxma, B., Voncken, F., Jannink, S., van Alen, T., Akhmanova, A., van Weelden, S.W., van Hellemond, J.J., Ricard, G., Huynen, M., Tielens, A.G., and Hackstein, J.H. (2004) The anaerobic chytridiomycete fungus *Piromyces* sp. E2 produces ethanol via pyruvate:formate lyase and an alcohol dehydrogenase E. *Mol. Microbiol.* **51**, 1389-1399
35. Kawata, T., Masuda, K., and Yoshino, K. (1975) Presence of fine spirals (spirosomes) in *Lactobacillus fermenti* and *Lactobacillus casei. Japan J Microbiol*. **19**, 225-227
36. Kessler, D., Leibrecht, I., and Knappe, J. (1991) Pyruvate-formate-lyase-deactivase and acetyl-CoA reductase activities of *Escherichia coli* reside on a polymeric protein particle encoded by adhE. *FEBS Lett*. **281**, 59-63
37. Laurenceau, R., Krasteva, P.V., Diallo, A., Ouarti, S., Duchateau, M., Malosse, C., Chamot-Rooke, J., and Fronzes, R. (2015) Conserved *Streptococcus pneumoniae* spirosomes suggest a single type of transformation pilus in competence. *PloS Pathog*. **11**(4):e1004835

38. Hsieh, S.I., Castruita, M., Malasarn, D., Urzica, E., Erde, J., Page, M.D., Yamasaki, H., Casero, D., Pellegrini, M., Merchant, S.S., and Loo, J.A. (2013) The proteome of copper, iron, zinc, and manganese micronutrient deficiency in *Chlamydomonas reinhardtii*. *Mol. Cell. Proteomics.* **12**, 65-86
39. Ball, S.G., Dirick, L., Decq, A., Martiat, J.C., and Matagne, R.F. (1990) Physiology of starch storage in the monocellular alga *Chlamydomonas reinhardtii*. *Plant Sci.* **66**, 1-9
40. Schmöllinger, S., Mühlhaus, T., Boyle, N.R., Blaby, I.K., Casero, D., Mettler, T., Moseley, J.L., Kropat, J., Sommer, F., Strenkert, D., Hemme, D., Pellegrini, M., Grossman, A.R., Stitt, M., Schroda, M., and Merchant, S.S. (2014) Nitrogen-sparing mechanisms in *Chlamydomonas* affect the Transcriptome, the proteome, and photosynthetic metabolism. *Plant Cell.* **26**, 1410-1435
41. Valledor, L., Furuhashi, T., Recuenco-Muñoz, L., Wienkoop, S., and Weckwerth, W. (2014) System-level network analysis of nitrogen starvation and recovery in *Chlamydomonas reinhardtii* reveals potential new targets for increased lipid accumulation. *Biotechnol Biofuels.* **7**, 171
42. Zabawinski, C., Van Den Koornhuyse, N., D'Hulst, C., Schlichting, R., Giersch, C., Delrue, B., Lacroix, J.M., Preiss, J., and Ball, S. (2001) Starchless mutants of *Chlamydomonas reinhardtii* lack the small subunit of a heterotetrameric ADP-glucose pyrophosphorylase. *J. Bacteriol.* **183**, 1069-1077
43. Malasarn, D., Kropat, J., Hsieh, S.I., Finazzi, G., Casero, D., Loo, J.A., Pellegrini, M., Wollman F.A., and Merchant, S.S. (2013) Zinc deficiency impacts CO2 assimilation and disrupts copper homeostasis in *Chlamydomonas reinhardtii*. *J. Biol. Chem.* **288**, 10672-10683
44. Wang, Y., Duanmu, D., and Spalding, M.H. (2011) Carbon dioxide concentrating mechanism in *Chlamydomonas reinhardtii*: inorganic carbon transport and CO_2 recapture. *Photosynth Res.* **109**, 115-122
45. Moroney, J.V., Husic, H.D., Tolbert, N.E., Kitayama, M., Manuel, L.J., and Togasaki, R.K. (1989) Isolation and characterization of a mutant of *Chlamydomonas reinhardtii* deficient in the CO(2) concentrating mechanism. *Plant Physiol.* **89**, 897-903
46. Fukuzawa, H., Miura, K., Ishizaki, K., Kucho, K.I., Saito, T., Kohinata, T. and Ohyama, K. (2001) Ccm1, a regulatory gene controlling the induction of a carbon-concentrating mechanism in *Chlamydomonas reinhardtii* by sensing CO2 availability. *Proc Natl Acad Sci USA.* **98**, 5347-5352
47. Karlsson, J., Clarke, A.K., Chen, Z.Y., Hugghins, S.Y., Park, Y.I., Husic, H.D., Moroney, J.V., and Samuelsson, G. (1998) A novel α-type carbonic anhydrase associated with the thylakoid membrane in *Chlamydomonas reinhardtii* is required for growth at ambient CO2. *EMBO J.* **17**, 1208-1216
48. Johnson, X., Wostrikoff, K., Finazzi, G., Kuras, R., Schwarz, C., Bujaldon, S., Nickelsen, J., Stern, D.B., Wollman, F.A., and Vallon, O. (2010) MRL1, a conserved Pentatricopeptide repeat protein, is required for stabilization of rbcL mRNA in *Chlamydomonas* and *Arabidopsis*. *Plant Cell.* **22**, 234-248
49. Johnson, X., Steinbeck, J., Dent, R.M., Takahashi, H., Richaud, P., Ozawa, S., Houille-Vernes, L., Petroutsos, D., Rappaport, F., Grossman, A.R., Niyogi, K.K., Hippler, M., and Alric, J. (2014) Proton gradient regulation 5-mediated cyclic electron flow under ATP- or redox-limited conditions: a study of ΔATpase pgr5 and ΔrbcL pgr5 mutants in the green alga *Chlamydomonas reinhardtii*. *Plant Physiol.* **165,** 438-452
50. Kucho, K., Yoshioka, S., Taniguchi, F., Ohyama, K., and Fukuzawa, H. (2003) Cis-acting elements and DNA-binding proteins involved in CO2-responsive transcriptional activation of Cah1 encoding a periplasmic carbonic anhydrase in *Chlamydomonas reinhardtii*. *Plant Physiol.* **133**, 783-793
51. Dagan, T., Roettger, M., Stucken, K., Landan, G., Koch, R., Major, P., Gould, S.B., Goremykin, V.V., Rippka, R., Tandeau de Marsac, N., Gugger, M., Lockhart, P.J., Allen, J.F., Brune, I., Maus, I., Pühler, A. and Martin, W.F. (2014) Genomes of Stigonematalean cyanobacteria (subsection V) and the evolution of oxygenic photosynthesis from prokaryotes to plastids. *Genome Biol. Evol.* **5**, 31-44
52. Keeling, P.J. (2010) The endosymbiotic origin, diversification and fate of plastids. *Philos. Trans. R. Soc. Lond. B. Biol. Sci.* **365**, 729-748

53. Cabiscol, E., Aguilar, J., and Ros, J. (1994) Metal-catalyzed oxidation of Fe2+ dehydrogenases. Consensus target sequence between propanediol oxidoreductase of Escherichia coli and alcohol dehydrogenase II of *Zymomonas mobilis*. *J. Biol. Chem*. **269,** 6592-6597
54. Leonardo, M.R., Cunningham, P.R., and Clark, D.P. (1993) Anaerobic regulation of the adhE gene, encoding the fermentative alcohol dehydrogenase of Escherichia coli. *J. Bacteriol*. **175**, 870-878
55. Pagels, M., Fuchs, S., Pané-Farré, J., Kohler, C., Menschner, L., Hecker, M., McNamarra, P.J., Bauer, M.C., von Wachenfeldt, C., Liebeke, M., Lalk, M., Sander, G., von Eiff, C., Proctor, R.A., and Engelmann, S. (2010) Redox sensing by a Rex-family repressor is involved in the regulation of anaerobic gene expression in Staphylococcus aureus. *Mol. Microbiol*. **76**, 1142-1161
56. Steunou, AS., Bhaya, D., Bateson, M.M., Melendrez, M.C., Ward, D.M., Brecht, E., Peters, J.W., Kühl, M., and Grossman, A.R. (2006) In situ analysis of nitrogen fixation and metabolic switching in unicellular thermophilic cyanobacteria inhabiting hot spring microbial mats. *Proc Natl Acad Sci USA*. **103**, 2398-2403
57. Beckham, K.S., Connolly, J.P., Ritchie, J.M., Wang, D., Gawthorne, J.A., Tahoun, A., Gally, D.L., Burgess, K., Burchmore, R.J., Smith, B.O., Beatson, S.A., Byron, O., Wolfe, A.J., Douce, G.R., and Roe, A.J. (2014) The metabolic enzyme AdhE controls the virulence of Escherichia coli O157:H7. *Mol Microbiol*. **93**, 199-211
58. Shasmal, M., Dey, S., Shaikh, T.R., Bhakta, S., and Sengupta, J. (2016) E. coli metabolic protein aldehyde-alcohol dehydrogenase-E binds to the ribosome: a unique moonlighting action revealed. *Sci Rep*. **6**, 19936
59. Harris, E. (1989). The *Chlamydomonas* Sourcebook: A Comprehensive Guide to Biology and Laboratory Use. Academic Press, San Diego.
60. van Lis, R., Atteia, A., Nogaj, L.A., and Beale, S.I. (2005) Subcellular localization and light-regulated expression of protoporphyrinogen IX oxidase and ferrochelatase in *Chlamydomonas reinhardtii*. *Plant Physiol*. **139**, 1946-1958
61. Goodstein, D.M., Shu, S., Howson, R., Neupane, R., Hayes, R.D., Fazo, J., Mitros, T., Dirks, W., Hellsten, U., Putnam, N., and Rokhsar, D.S. (2012). Phytozome: a comparative platform for green plant genomics. *Nucleic Acids Res*. **40**, D1178-1186
62. Dupierris, V, Masselon, C, Court, M, Kieffer-Jaquinod, S., and Bruley, C. (2009) A toolbox for validation of mass spectrometry peptides identification and generation of database: IRMa. *Bioinformatics*. **25**, 1980-1981
63. Wessel, D., and Flügge, U.I. (1984) A method for the quantitative recovery of protein in dilute solution in the presence of detergents and lipids. *Anal Biochem*. **138**, 141-143
64. Durrant, I. (1990) Light-based detection of biomolecules. *Nature*. **346**, 297-298
65. Studier, F.W. (2005) Protein production by auto-induction in high-density shaking cultures. Prot. Exp. Purif. **41**, 207-234.
66. O'Toole, E.T. (2010) *Chlamydomonas* cryopreparation methods for the 3-D analysis of cellular organelles. *Methods Cell Biol*. **96**, 71-91
67. Montella, C., Bellsolell, L., Pérez-Luque, R., Badía, J., Baldoma, L., Coll, M., and Aguilar, J. (2005) Crystal structure of an iron-dependent group III dehydrogenase that interconverts L-lactaldehyde and L-1,2-propanediol in *Escherichia coli*. *J Bacteriol*. **187**, 4957-4966
68. Zheng, T., Olson, D.G., Tian, L., Bomble, Y.J., Himmel, M.E., Lo, J., Hon, S., Shaw, A.J., van Dijken, J.P., and Lynd, L.R. (2015) Cofactor specificity of the bifunctional alcohol and aldehyde dehydrogenase (AdhE) in wild-type and mutant Clostridium thermocellum and Thermoanaerobacterium saccharolyticum. *J. Bacteriol*. **197**, 2610-2619

TABLES

Table 1. Distribution of ADHE among the five eukaryotic supergroups defined by Adl et al. (2012) (26).

SUPERGROUP		Species name	Lifestyle	% identity*	Accession number
Archaeplastida	Chlorophytes	*Chlamydomonas reinhardtii*	Free-living photosythetic alga	_	gi|92084840
	Chlorophytes	*Volvox carteri*	Free-living photosythetic alga	84	gi|302853679
	Chlorophytes	*Chlorella variabilis*	Free-living photosythetic alga	68	gi|552841275
Amoebozoa	Entamoebids	*Entamoeba histolytica*	Human pathogen (intestine)	47	gi|2492737
	Pelobionts	*Mastigamoeba*	Free-living species	55	gi|21435953
Excavata	Diplomonads	*Giardia intestinalis*	Human pathogen (intestine)	52	gi|2052472
	Diplomonads	*Spironucleus barkhanus*	Fish pathogen	53	gi|27983190
Opisthokonta	Fungi (chytrid)	*Neocallimastix frontalis*	Anaerobic rumen fungus	52	gi|387233067
	Fungi (chytrid)	*Piromyces* sp. E2	Anaerobic rumen fungus	52	gi|33578055
	Fungi	*Togninia minima UCRPA7*	Grapevine pathogen	47	gi|631237462
SAR	Cryptophytes	*Guillardia theta CCMP2712*	Free-living photosythetic alga	47	gi|551672365
	Cercozoa	*Bigelowiella natans CCMP2755*	Free-living photosythetic alga	43	jgi|Bigna1|85335
	Apicomplexa	*Cryptosporidium hominis TU502*	Anaerobic pathogen	48	gi|67623585

SAR, Stramenopiles, Alveolata, Rhizaria. *, amino acid identity with *C. reinhardtii* ADHE.

Table 2. Enzymatic data on the recombinant ADHE.

Reaction #	V_{max} $\mu mol.min^{-1}.mg^{-1}$	pH_{max}
1	0.88 ± 0.18	6.5-7.0
1 (+Fe)	1.07 ± 0.09	
2	4.00 ± 0.63	6.5-7.0
2 (+Fe)	4.99 ± 1.21	
3	0.85 ± 0.06	
3 (+Fe)	1.20 ± 0.40	
4	0.69 ± 0.29	
4 (+Fe)	0.83 ± 0.33	

Standard reaction medium contains 50 mM potassium phosphate (pH 7.0). The substrates were used at the following concentrations: NAD (1.5 mM), NADH (0.4 mM), acetyl-CoA (100 µM), Coenzyme A (100 µM), ethanol (200 mM), acetaldehyde 1 mM). Fe, incubation with 0.3 mM $FeCl_3$

Table 3. Km values of rADHE for the activities directed towards its physiological role, the production of ethanol.

Reaction #	Substrate	Km
1	NADH	120.9 ± 48.0 µM
1	Acetyl-CoA	12.7 ± 2.9 µM
2	NADH	20.9 ± 3.5 µM
2	Acetaldehyde	35.0 ± 17.6 mM

Table 4. Relative abundance of ADHE and PFL in *Chlamydomonas* cells exposed to various physiological conditions.

Strain	Phenotype	Medium	Light intensity	ADHE relative	PFL relative
CC-124	WT	TAP	10-15 µE	1	1
CC-124	WT	TAP	40-50 µE	1	1
CC-124	WT	TAP	200 µE	1,6-1,8	1,1-1,2
CC-124	WT	HSM + 2% CO2	40-50 µE	0,3	nd
CC-124	WT	TAP+DCMU	40-50 µE	0,9-1,2	1,3-1,6
CC-124	WT	TAP (no ZnSO4)	40-50 µE	3,3-3,5	1,5-1,7
CC124	WT	N-free TAP (24h)	40-50 µE	2,5	0,75
10-6C	Lacks RubisCO carboxylase activity	TAP	40-50 µE	3,4-3,6	1,4-1,6
10-6C	Lacks RubisCO carboxylase activity	TAP (no ZnSO4)	40-50 µE	3,3-3,5	nd
ΔRBCL	Lacks RubisCO	TAP	10-15 µE	0,2-0,3	1,1-1,4
CIA3	Lacks carbonic anhydrase 3	TAP	40-50 µE	1,4-1,7	1,1-1,4
CIA5	Lacks CCM1	TAP	40-50 µE	1,5-1,7	1,1-1,3
sta6	Impaired in starch synthesis	TAP (no ZnSO4)	40-50 µE	1,0-1,1	nd
sta6	Impaired in starch synthesis	TAP (no ZnSO4)	40-50 µE	3,0-3,2	nd

FIGURES

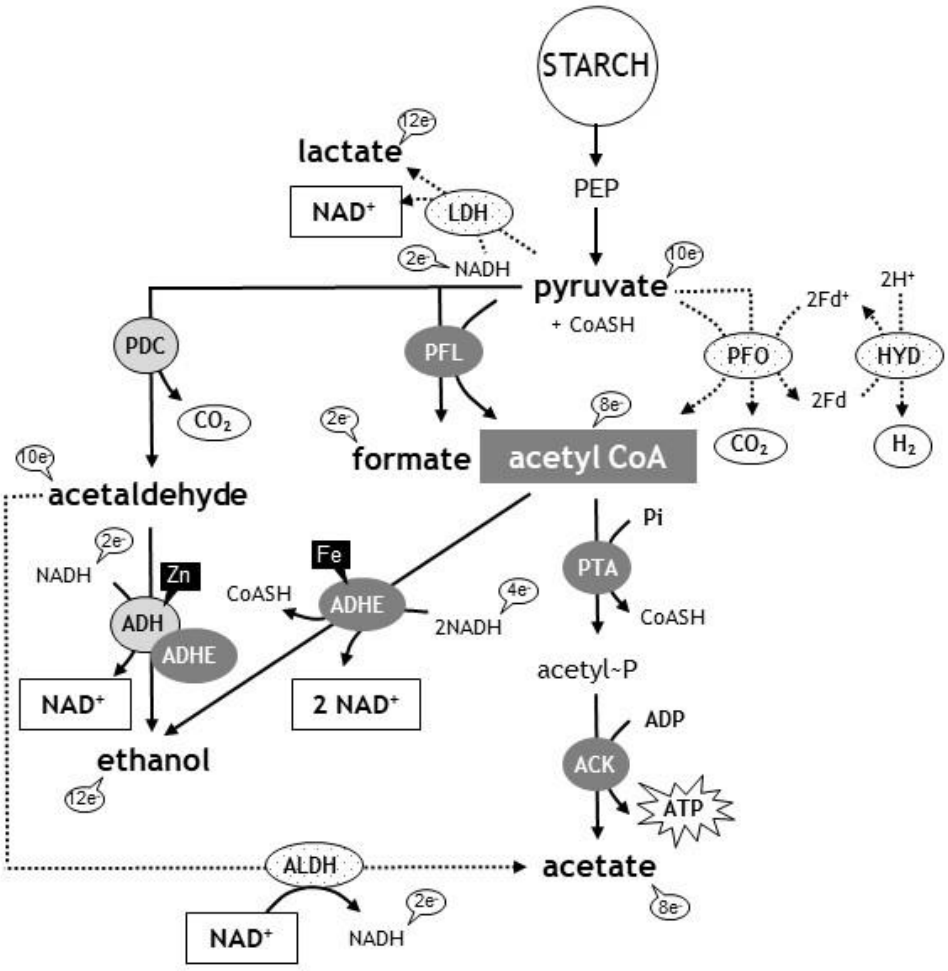

FIGURE 1. Anaerobic metabolic routes in *Chlamydomonas*. Under dark anoxia, starch is metabolized to pyruvate via glycolysis, thereby generating ATP and reducing power (NADH). The network shows a pyruvate branch point with four enzymes. Another branch point is acetyl-CoA that can be used to produce ethanol via ADHE or acetate via the PTA-ACK pathway. Network is simplified by the omission of the subcellular localization of the different enzymes. Fe and Zn, indicate the metal in the active site of the alcohol dehydrogenases. To better understand the metabolic responses, the number of oxidizable electrons is indicated for each metabolite. The main fermentation route used by the alga incubated in AIB under dark anoxia is the «PFL-gated pathway» which consists of PFL, ADHE and PTA-ACK indicated in dark grey.

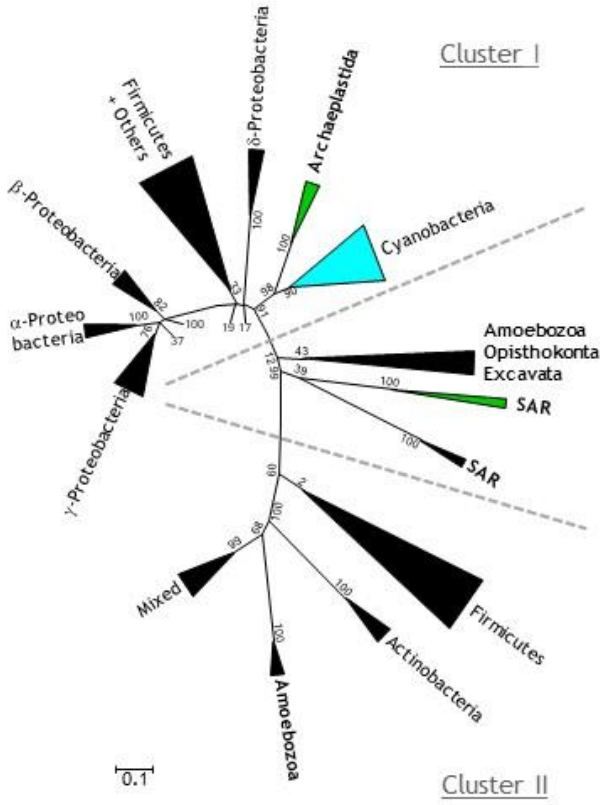

FIGURE 2. Schematic phylogenetic tree of aldehyde/alcohol dehydrogenase from bacterial and eukaryotic sources. The tree was constructed using the maximum likelihood algorithm. Eukaryotic supergroups are indicated in bold. Photosynthetic eukaryotes are indicated in green, cyanobacteria in blue. The list of species used in this analysis can be found in Supplemental Data Set 1. Multiple alignment is shown in Supplemental Data Set 2.

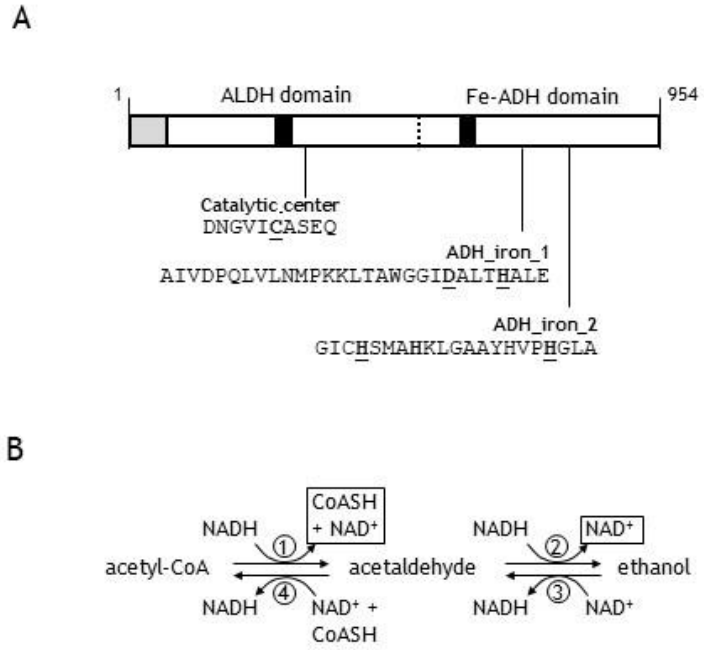

FIGURE 3. Structural and enzymatic characteristics of ADHE. A) The *Chlamydomonas* enzyme consists of an N-terminal aldehyde dehydrogenase (ALDH) domain (cd07077) followed by a C-terminal alcohol dehydrogenase (ADH) domain (cd08178). The catalytic Cys residue in the ALDH domain (Cys323) is indicated. Two signatures for iron-binding were identified in the ADH domain: ADH_iron_1 (residues 706-734) (Prosite PS00913) and ADH_iron_2 (residues 794-814)(Prosite PS00060). The position of the residues potentially involved in iron coordination (D727; H731; H797; H811) was inferred from the structure of the *E. coli* iron-dependent alcohol dehydrogenase FucO (67). Black boxes indicate NADH binding sites (G270-G291; E599-M622) based on (68). Compared to bacterial enzymes, the algal ADHE exhibits at its N-terminus an extension (grey box) which likely serves for intracellular targeting. B) Enzymatic activities catalyzed by ADHE.

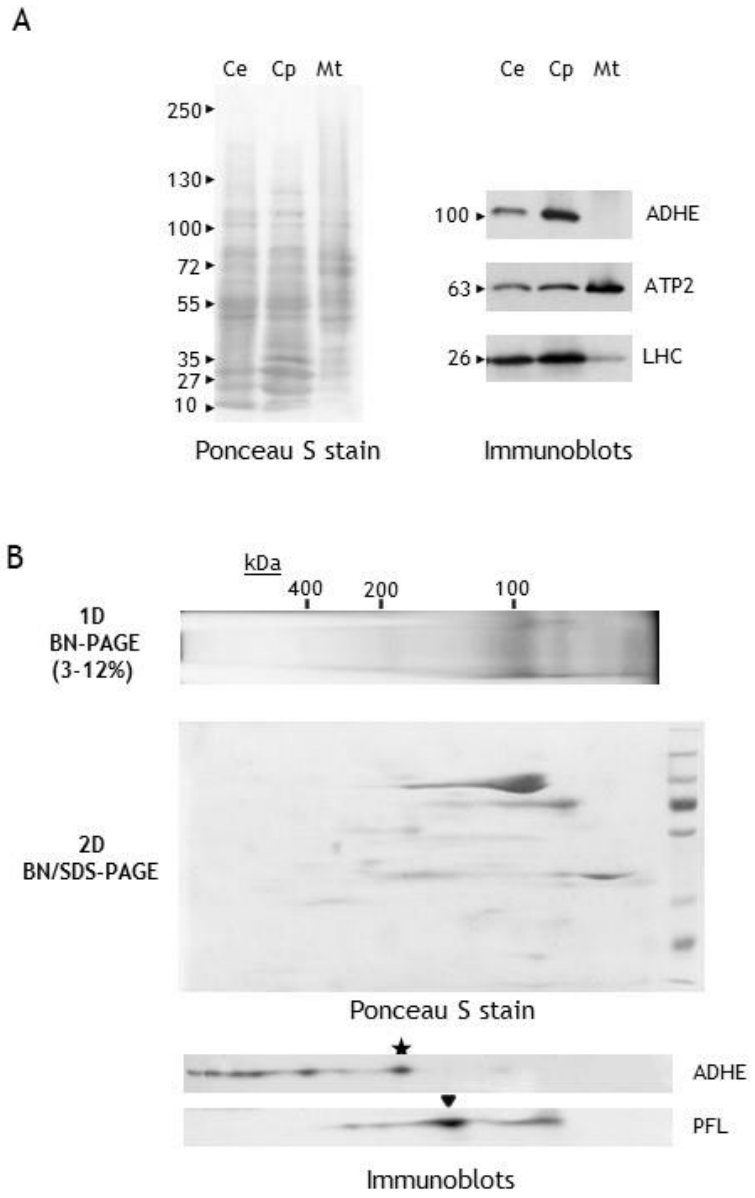

Figure 4A,B. ***Chlamydomonas*** **ADHE is located in the chloroplast stroma. A)** Organelle fractionation from strain 10-6C. Ce, cell extract; Cp, chloroplast fraction and Mt, mitochondrial fraction. Proteins were separated on SDS-PAGE (5-12% polyacrylamide gel). Immunoblots show the distribution in isolated organelles of light-harvesting complex proteins (LHC), subunit b of the mitochondrial F_0F_1-ATPase (ATP2), and ADHE. **B)** Two-dimensional resolution of proteins in a stromal fraction. Proteins were subjected to BN (3-12% acrylamide)/SDS-PAGE (10% acrylamide) and further transferred to nitrocellulose for immunodetection. ★, position of the ADHE dimer; ▼, position of the PFL dimer.

C

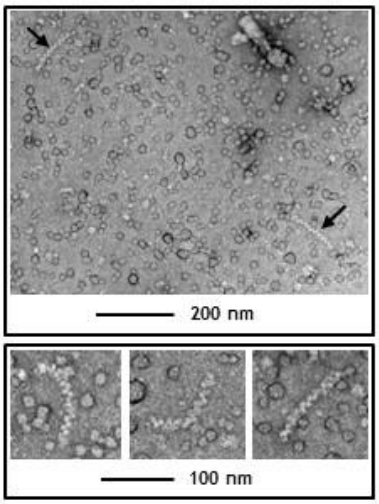

FIGURE 4C. *Chlamydomonas* ADHE is located in the chloroplast stroma. Electron micrograph images of a stromal protein fraction using uranyl acetate as negative stain.

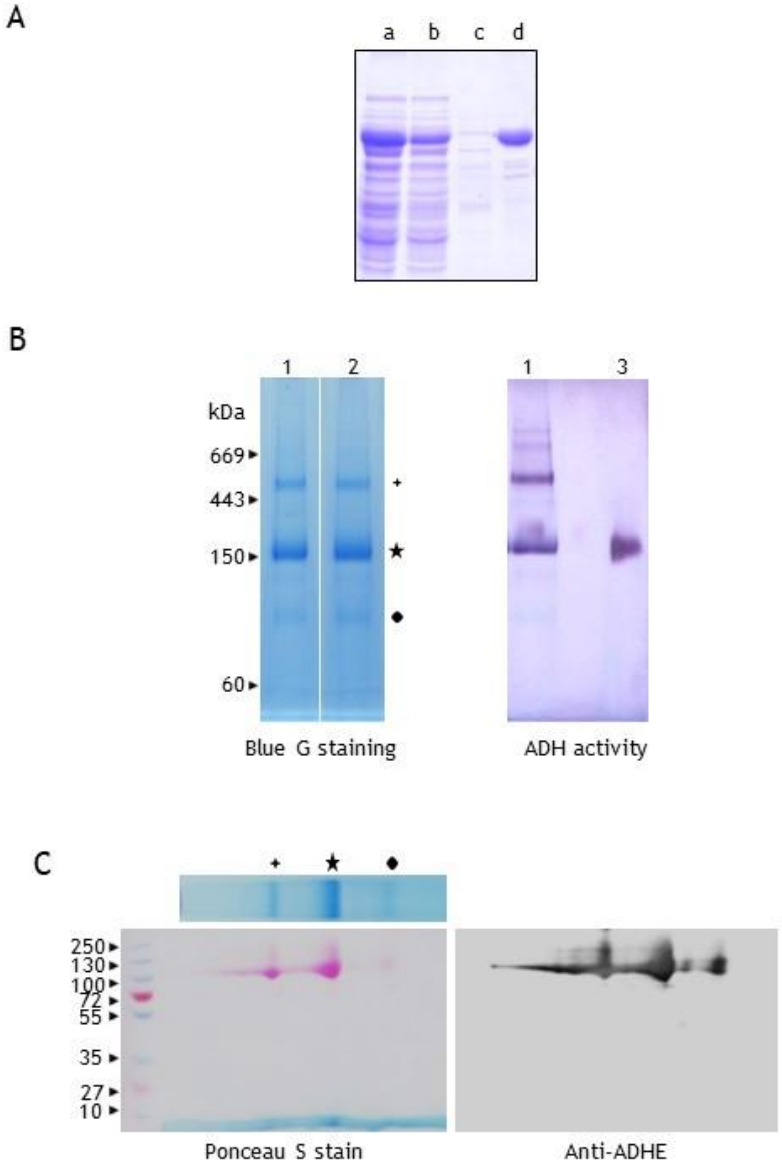

FIGURE 5. PAGE analysis of *Chlamydomonas* recombinant ADHE. A) Purification of His-tagged *Chlamydomonas* ADHE (rADHE). Fractions were analyzed on SDS-PAGE (10% acrylamide). a) *E. coli* soluble fraction, b) flow-through, c) 10 mM imidazole wash, d) rADHE eluted with 100 mM imidazole (~10 µg). **B)** Freshly purified rADHE (25µG) was subjected to BN-PAGE (3-12% acrylamide). 1) rADHE was purified under anaerobic conditions, 2) rADHE was purified under atmospheric conditions, 3) *S. cerevisiae* ADH1 (0,5 µG). **C)** Detection of different forms of rADHE by immunoblotting after two-dimensional BN/SDS-PAGE. One BN gel lane was excised, subjected to denaturation in 1% SDS and 1% β-mercaptoethanol and loaded on a 10% acrylamide gel. Proteins were then transferred to a nitrocellulose membrane, stained with Ponceau S and probed for ADHE.

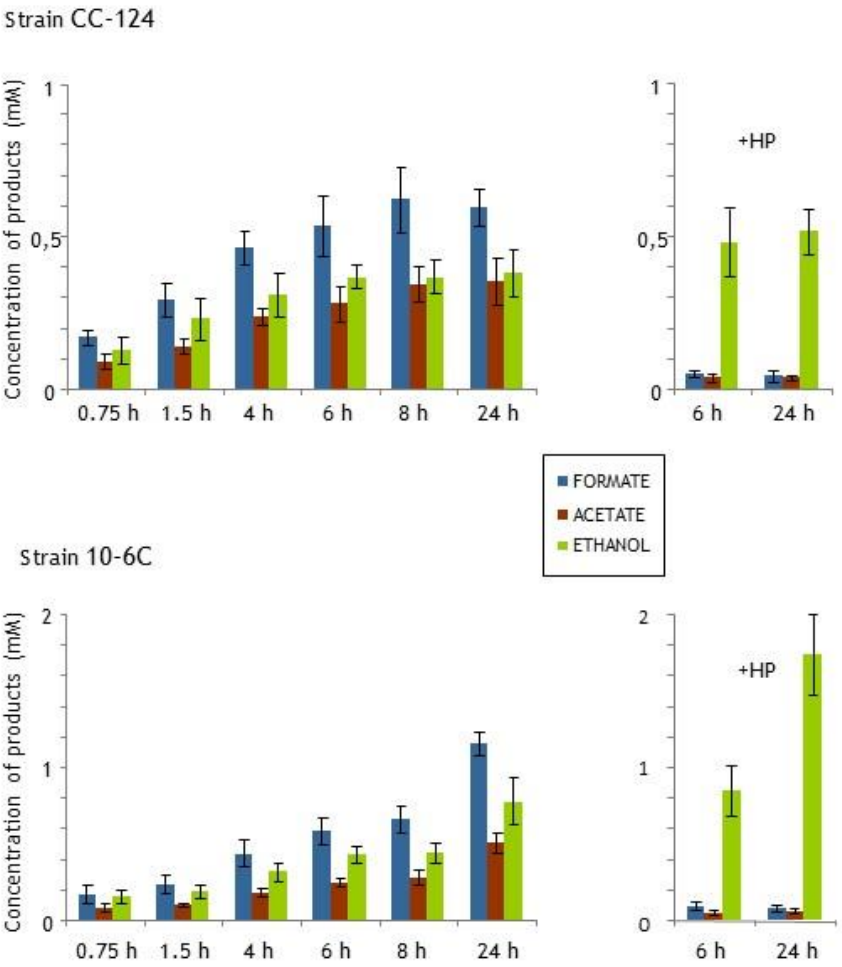

FIGURE 6. Profiles of fermentative products in *Chlamydomonas* incubated in dark anoxia. Kinetics of acetate, formate and ethanol production by the wild-type strain (upper graph) and the mutant strain (lower graph). Metabolites in the extracellular medium were identified by HPLC at the indicated times. HP, indicates that 10 mM sodium hypophosphite was added to the incubation medium to inhibit PFL. Metabolite productions are expressed in mM in cell suspension at 10^7 cells mL^{-1}. Each value is the mean of at least 4 independent experiments carried out with cell suspension of similar concentration (~10^7 cells mL^{-1}). The error bars indicate standard deviations. Note the different scales for the two strains.

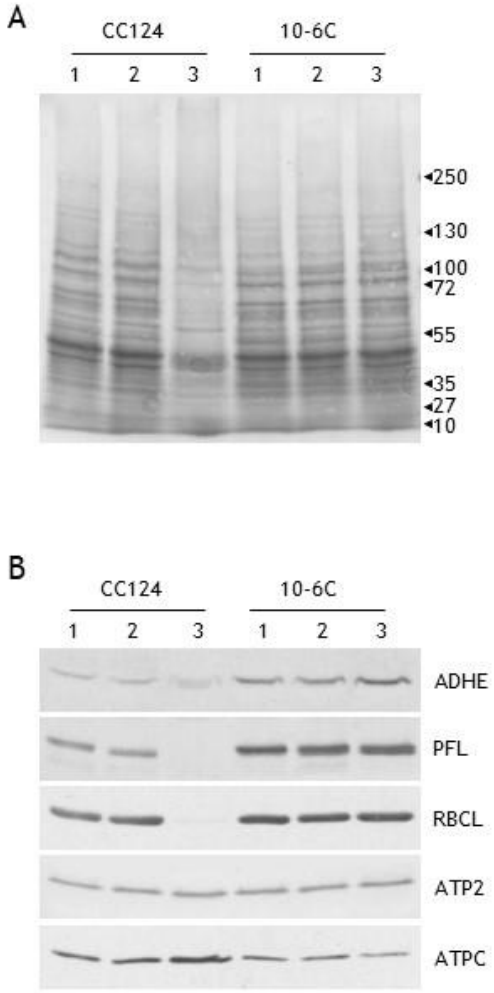

FIGURE 7. Protein abundance in response to dark anoxia in strains CC-124 (wild-type) and 10-6C (lacks RubisCO carboxylase activity). Cells were kept under dark anoxia in AIB medium at a cell concentration of 10^7 cells mL^{-1}. Protein in cell extracts were separated by urea/SDS-PAGE (6M urea/5-12% acrylamide) and transferred to nitrocellulose membrane. *Lane 1*, exponentially grown cells; *lane 2*, 6 h incubation; *lane 3*, 24 h incubation. A) Nitrocellulose membrane was stained with Ponceau red S. B) Selected proteins were detected by immunoblot analyses with antisera against aldehyde/alcohol dehydrogenase (ADHE), pyruvate formate lyase (PFL), large subunit of RubisCO (RBCL), subunit b of mitochondrial ATPase (ATP2) and subunit gmma of chloroplast ATPase (ATPC). Note that strain 10-6C exhibits higher levels of ADHE and PFL.

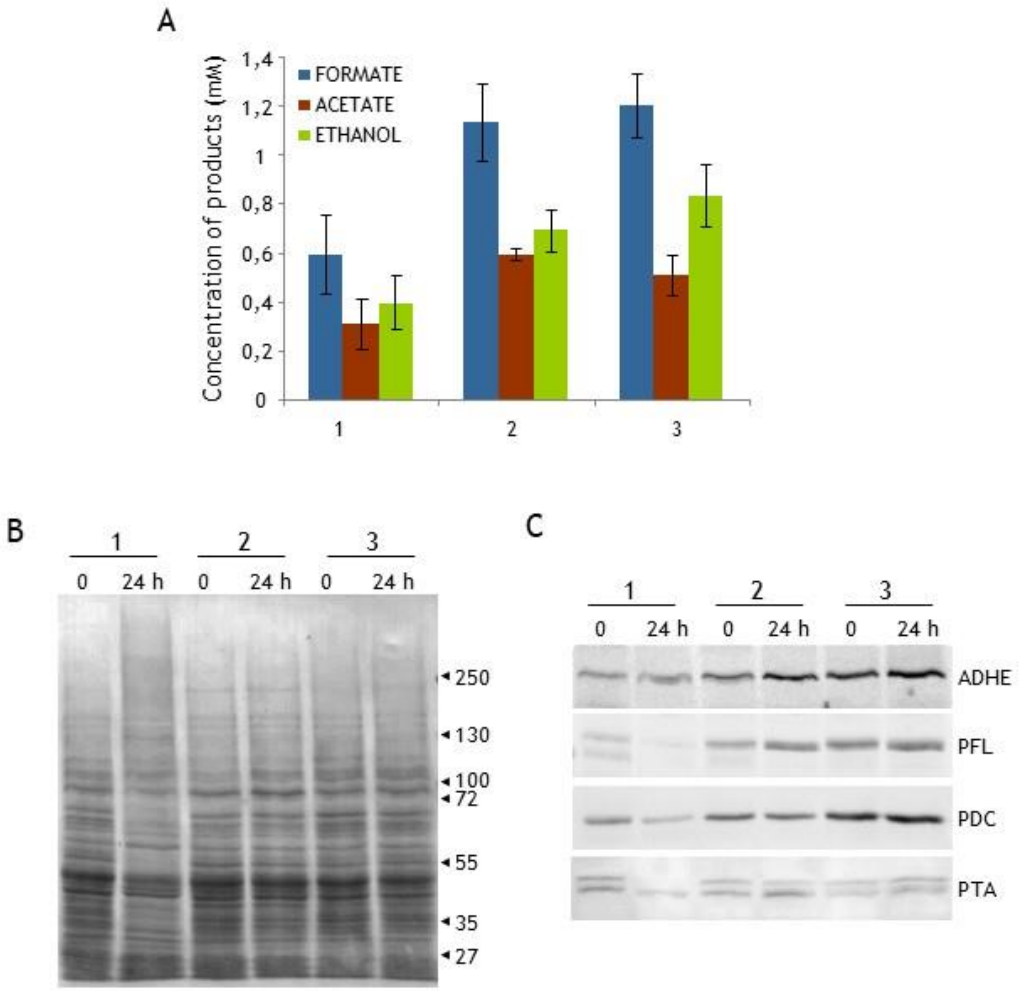

FIGURE 8. Fermentation by zinc-deficient cells. Cells were incubated for 24 h under dark anoxia in AIB medium, at a concentration of 10^7 cells mL^{-1}. *Sample 1*, strain CC-124 grown on TAP medium; *sample 2*, strain CC-124 grown on zinc-deficient TAP medium, and *sample 3*, strain 10-6C grown on TAP medium. (**A**) Fermentation products excreted after 24 h in dark anoxia. Metabolite concentrations are given for 10^7 cells mL^{-1}. (B,C) Proteins in extracts from cells before (t=0) and after a prolonged incubation in anoxia (t=24 h) were analysed on urea/SDS-PAGE urea/SDS-PAGE (6M urea/5-12% acrylamide) and transferred to nitrocellulose membrane. (**B**) Ponceau S stained nitrocellulose membrane. (**C**) Immunoblots showing the levels of specific fermentative enzymes. The two bands detected by the anti-PTA serum likely correspond to the chloroplast and mitochondrial isoforms of phosphotransacetylase (see Supplemental Fig. s S6, S7).

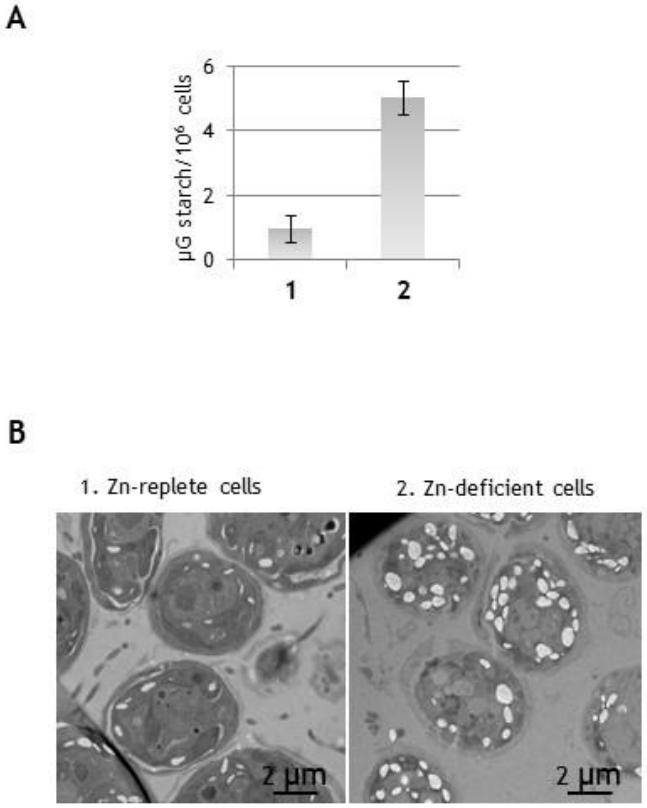

Figure 9. Impact of zinc on starch accumulation. **A**) Starch content in exponentially growing cells (strain CC-124). The data are the means of at least three independent replicates. **B**) Electron micrographs of cell sections showing higher content in starch cells deficient in zinc compared to cells grown in presence of zinc.

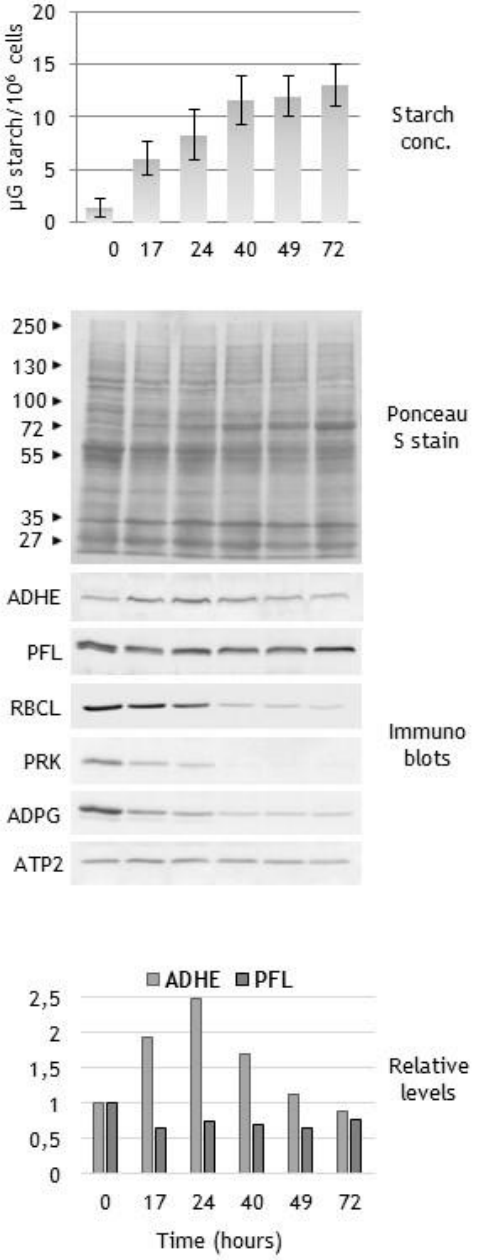

Figure 10. ADHE levels increase upon exposure to nitrogen starvation conditions. Starch content and select proteins were analysed after transfer of *Chlamydomonas* CC-124 strain to N free TAP medium.

SUPPLEMENTARY INFORMATION

Concerted upregulation of bifunctional aldehyde/alcohol dehydrogenase (ADHE) and starch content in *Chlamydomonas* cells allows increased survival in prolonged dark anoxia.

Robert van Lis[1,2], Marion Popek[1], Yohann Couté[3,4,5], Artemis Kosta[6], Dominique Drapier[7], Wolfgang Nitschke[1] and Ariane Atteia[1,†]

[1]Aix Marseille Univ, CNRS, the Unité de Bioénergétique et Ingénierie des Protéines-UMR 7281, 31 Chemin Joseph Aiguier, F-13402 Marseille, France
[2]INRA, Laboratoire de Biotechnologie de l'Environnement, Narbonne, France

[3]Université Grenoble Alpes, BIG-BGE, F-38000 Grenoble, France
[4]Commissariat à l'Energie Atomique, BIG-BGE, F-38000 Grenoble, France
[5]INSERM, BGE, F-38000 Grenoble, France
[6]Microscopy core facility, FR3479 Institut de Microbiologie de la Méditerranée 31 chemin Joseph Aiguier, 13402 Marseille cedex 20, France
[7]UMR 7141, CNRS and Université Pierre et Marie Curie (UPMC - Paris 06), Institut de Biologie Physico-Chimique, 13 rue Pierre et Marie Curie, F-75005 Paris, France

Supplemental Data Set 1. Species used for the phylogenetic analysis presented in Figure 2
Supplemental Data Set 2. Multiple sequence alignment of ADHEs.

Supplemental Figures:
FIGURE S1. Specificity of the anti-ADHE serum.
FIGURE S2. RBCL of *Chlamydomonas* strain 10-6C: identification by mass spectrometry.
FIGURE S3. Identification of *Chlamydomonas* ADHE by mass spectrometry.
FIGURE S4. Immunoblot analysis of cells incubated in dark anoxia in presence of sodium hypophosphite, an inhibitor of PFL.
FIGURE S5. ADHE abundance in conditions of zinc-deficiency.
FIGURE S6. Production of antibodies to *Chlamydomonas* phosphotransacetylases.
FIGURE S7. Identification of *Chlamydomonas* PTAs by mass spectrometry.

FIGURE S1. Specificity of the anti-ADHE serum.
Proteins were separated on SDS-PAGE (5-12% acrylamide) and transferred to nitrocellulose membrane. *Lane 1*, recombinant ADHE (0.15 µg); *lane 2*, cell extract from wild-type strain CC-124 (40 µg proteins); *lane 3*, cell extract from mutant strain 10-6C (40 µg proteins). Left: membrane was stained with Ponceau red S; right: membrane was probed for ADHE, using the anti-ADHE antibodies at a dilution of 1:2,500.

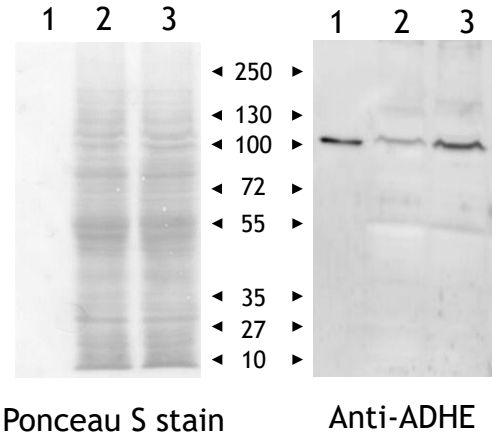

FIGURE S2. RBCL in *Chlamydomonas* strain 10-6C: identification by mass spectrometry. Chloroplasts from strain 10-6C were loaded on a urea/SDS-PAGE. The gel piece in the 40-kDa region was subjected to nanoLC-MS/MS analysis.

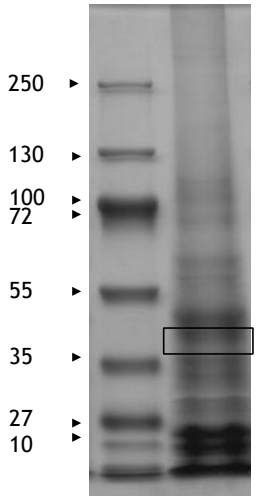

Sequence alignment of wild-type and mutant RBCLs. Tryptic peptides that match mutated RBCL protein are indicated, including the peptide that covers the mutation (Gly -> Asp).

```
Wild-type       MVPQTETKAGAGFKAGVKDYRLTYYTPDYVVRDTDILAAFRMTPQPGVPPEECGAAVAAE
Mutant          MVPQTETKAGAGFKAGVKDYRLTYYTPDYVVRDTDILAAFRMTPQPGVPPEECGAAVAAE
                ************************************************************

Wild-type       SSTGTWTTVWTDGLTSLDRYKGRCYDIEPVPGEDNQYIAYVAYPIDLFEEGSVTNMFTSI
Mutant          SSTGTWTTVWTDGLTSLDRYKGRCYDIEPVPGEDNQYIAYVAYPIDLFEEGSVTNMFTSI
                ************************************************************

Wild-type       VGNVFGFKALRALRLEDLRIPPAYVKTFVGPPHGIQVERDKLNKYGRGLLGCTIKPKLGL
Mutant          VGNVFGFKALRALRLEDLRIPPAYVKTFVGPPHGIQVERDKLNKYGRGLLDCTIKPKLGL
                ************************************************ *********

Wild-type       SAKNYGRAVYECLRGGLDFTKDDENVNSQPFMRWRDRFLFVAEAIYKAQAETGEVKGHYL
Mutant          SAKNYGRAVYECLRGGLDFTKDDENVNSQPFMRWRDRFLFVAEAIYKAQAETGEVKGHYL
                ************************************************************

Wild-type       NATAGTCEEMMKRAVCAKELGVPIIMHDYLTGGFTANTSLAIYCRDNGLLLHIHRAMHAV
Mutant          NATAGTCEEMMKRAVCAKELGVPIIMHDYLTGGFTANTSLAIYCRDNGLLLHIHRAMHAV
                ************************************************************

Wild-type       IDRQRNHGIHFRVLAKALRMSGGDHLHSGTVVGKLEGEREVTLGFVDLMRDDYVEKDRSR
Mutant          IDRQRNHGIHFRVLAKALRMSGGDHLHSGTVVGKLEGEREVTLGFVDLMRDDYVEKDRSR
                ************************************************************

Wild-type       GIYFTQDWCSMPGVMPVASGGIHVWHMPALVEIFGDDACLQFGGGTLGHPWGNAPGAAAN
Mutant          GIYFTQDWCSMPGVMPVASGGIHVWHMPALVEIFGDDACLQFGGGTLGHPWGNAPGAAAN
                ************************************************************

Wild-type       RVALEACTQARNEGRDLAREGGDVIRSACKWSPELAAACEVWKEIKFEFDTIDK
Mutant          RVALEACTQARNEGRDLAREGGDVIRSACKWSPELAAACEVWKEIKFEFDTIDK
                ********************************************************
```

FIGURE S3. Identification of *Chlamydomonas* ADHE by mass spectrometry
•List of the tryptic peptides that match the ADHE sequence (Phytozome accession number g18056). Peptides were identified in 3 independent nanoLC-MS/MS analyses: *gel band*: chloroplast proteins in 100-kDa region; *stacking 1,* chloroplast soluble proteins; and *stacking 2*, whole cells.

Peptide sequence	Position		gel band		stacking 1		stacking 2	
	Start	Stop	Spectral Count	Highest score	Spectral Count	Highest score	Spectral Count	Highest score
AEAAAPVAAAPATPHAEVK	54	72	1	40.63	1	37.91		
AEAAAPVAAAPATPHAEVKK	54	73	2	41.53	1	46.61	1	25.64
ERAPATDEALTELK	74	87	1	69.03	2	62.75	2	63.27
APATDEALTELK	76	87	1	77.70	1	79.12	1	53.21
RAQTAQAQYSTYTQEQVDEIFR	92	113			1	53.60		
AQTAQAQYSTYTQEQVDEIFR	93	113	1	136.06	2	104.36	2	119.00
NHFASEFIYNK	146	156	1	61.34	1	60.90	2	54.80
TCGVIEHDPAGGIQK	162	176	2	88.75	2	96.77	2	83.08
VAEPVGVIAGIVPTTNPTSTAIFK	177	200	2	71.88	2	58.46	1	32.24
NALVLCPHPR	209	218					1	44.21
AAYSSGNPSLGVGAGNTPALIDETADVAMAVSSILLSK	278	315	1	25.53	1	33.28		
TFDNGVICASEQSVVVVAK	316	334			1	98.25	1	91.52
RGAYFLTEDDKVK	346	358	1	47.37			1	40.16
GAYFLTEDDKVK	347	358	1	73.87	1	51.59	1	48.91
LNPNIVGQSIPK	369	380	1	83.04	1	69.30	1	72.70
LAALFGIK	381	388	1	55.48	1	50.57	2	43.48
VLIGEVEK	395	402					1	36.45
VLIGEVEKIGPEEALSQEK	395	413	1	39.44				
IGPEEALSQEK	403	413	1	59.36	2	40.93	3	64.23
LCPILAMYR	414	422	2	31.23				
MACELIMYGGAGHTSVLYTNPLNNAHIQQYQSAVK	432	466					3	27.58
ENMLWFR	525	531	1	35.84	1	36.86	1	26.61
GGCLEVALTDLR	540	551	1	94.51	2	95.03	2	86.84
AFIVTDKPLFDMGYADK	556	572			1	34.71	4	83.15
VTHILDSINVHHQVFYHVTPDPTLACIEAGLK	573	604					1	23.46
EILEFKPDVIIALGGGSPMDAAK	605	627					2	80.22
IMWLMYECPDTR	628	639	2	78.58	2	74.95	1	63.07
FDGLAMR	640	646	1	41.84	1	38.04		
VYEVPELGK	654	662			1	29.54		
KATMVCIPTTSGTGSEVTPFSVVTDER	663	689			1	42.89		
ATMVCIPTTSGTGSEVTPFSVVTDER	664	689	1	47.29	3	94.16	2	79.97
YPLADYALTPSMAIVDPQLVLNMPK	694	718	5	72.20	3	91.93	3	94.95
EAISLLFK	751	758	1	46.66	1	46.76	1	46.54
AYANGSNDYLAR	763	774					1	58.43
LGAAYHVPHGLANAALISHVIR	803	824	2	39.67				
YNATDMPAK	825	833	1	47.89	1	50.74	1	57.09
QAAFPQYEYPTAK	834	846	1	55.49	1	62.15	1	58.91
QDYADLANMLGLGGNTVDEK	847	866	3	117.60	4	133.25	3	100.77
LIEAVEELK	870	878					1	44.04
LIEAVEELKAK	870	880	2	62.52	1	45.87		
VDIPPTIK	881	888	1	25.51				
EIFNDPKVDADFLANVDALAEDAFDDQCTGANPR	889	922			1	48.55		
VDADFLANVDALAEDAFDDQCTGANPR	896	922	2	111.57	3	114.74	1	111.70
YPLMADLK	923	930	2	33.37			1	27.48
QLYLDAHAAPILPVK	931	945	2	64.38			2	54.53
TLEFFSK	946	952	1	29.82				

•**Tryptic peptides that match the ADHE sequence**. Peptides are highlighted in blue. Residues highlighted in black are those which differ between the phytozome sequence (here; T, V) and the sequence in PubMed (accession number: CAF04128; residues A, T). The identification of tryptic peptide "VLIGEVEK" confirms the phytozome sequence. The catalytic center in the ALDH as well as the signatures for iron-binding in the ADH domain (See Figure 1) are underlined.

```
   1 MMSSSLVSGKRVAVPSAAKPCAAVPLPRVAGRRTAARVVCEAAPSGAAPASPKAEAAAPV
  61 AAAPATPHAEVKKERAPATDEALTELKALLKRAQTAQAQYSTYTQEQVDEIFRAAAEAAN
 121 AARIPLAKMAVEETRMGVAEDKVVKNHFASEFIYNKYKHTKTCGVIEHDPAGGIQKVAEP
 181 VGVIAGIVPTTNPTSTAIFKSLLSLKTRNALVLCPHPRAAKSTIAAARIVRDAAVAAGAP
 241 PNIISWVETPSLPVSQALMQATEINLILATGGPAMVRAAYSSGNPSLGVGAGNTPALIDE
 301 TADVAMAVSSILLSKTFDNGVICASEQSVVVVAKAYDAVRTEFVRRGAYFLTEDDKVKVR
 361 AGVVVDGKLNPNIVGQSIPKLAALFGIKVPQGTKVLIGEVEKIGPEEALSQEKLCPILAM
 421 YRAPDYDHGVKMACELIMYGGAGHTSVLYTNPLNNAHIQQYQSAVKTVRILINTPASQGA
 481 IGDLYNFHLDPSLTLGCGTWGSTSVSTNVGPQHLLNIKTVTARRENMLWFRVPPKIYFKG
 541 GCLEVALTDLRGKSRAFIVTDKPLFDMGYADKVTHILDSINVHHQVFYHVTPDPTLACIE
 601 AGLKEILEFKPDVIIALGGGSPMDAAKIMWLMYECPDTRFDGLAMRFMDIRKRVYEVPEL
 661 GKKATMVCIPTTSGTGSEVTPFSVVTDERLGAKYPLADYALTPSMAIVDPQLVLNMPKKL
 721 TAWGGIDALTHALESYVSICATDYTKGLSREAISLLFKYLPRAYANGSNDYLAREKVHYA
 781 ATIAGMAFANAFLGICHSMAHKLGAAYHVPHGLANAALISHVIRYNATDMPAKQAAFPQY
 841 EYPTAKQDYADLANMLGLGGNTVDEKVIKLIEAVEELKAKVDIPPTIKEIFNDPKVDADF
 901 LANVDALAEDAFDDQCTGANPRYPLMADLKQLYLDAHAAPILPVKTLEFFSKIN
```

FIGURE S4. Immunoblot analysis of cells incubated in dark anoxia in presence of sodium hypophosphite, an inhibitor of PFL.

Proteins (40 µg) from dark anoxic cells were separated on urea/SDS-PAGE and transferred to nitrocellulose membrane. Detection of ADHE and PDC was performed by Western blotting. *Lane 1*, incubation for 6 h in AIB; *lane 2*, incubation for 24 h in AIB; *lane 3*, incubation 6 h in AIB supplemented with 10 mM $NaPO_2H_2$; *lane 4,* incubation 24 h in AIB supplemented with 10 mM $NaPO_2H_2$.

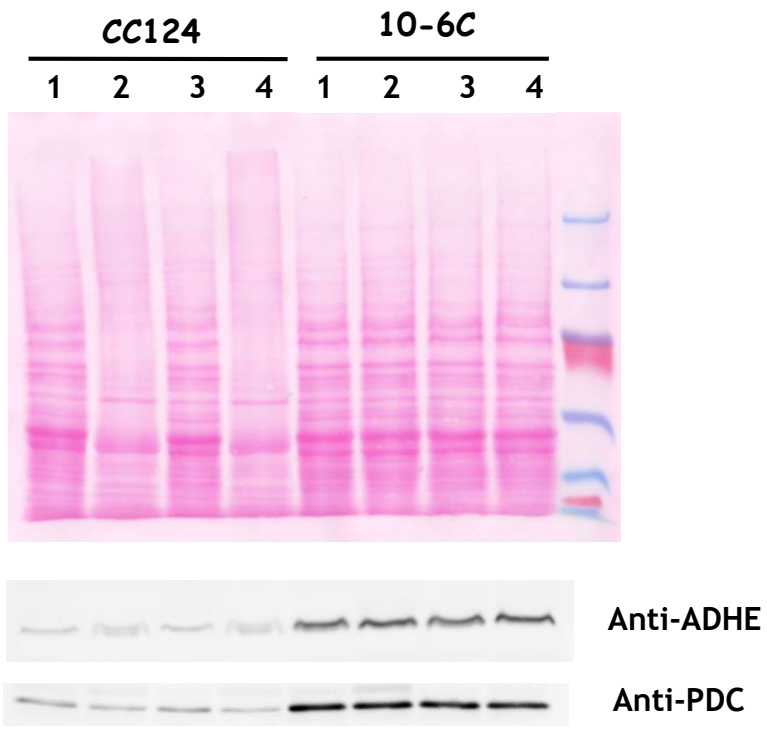

FIGURE S5. ADHE abundance in conditions of zinc-deficiency.
Protein analysis of cell extracts (40 µG). *Lane 1*, strain CC-124 grown on TAP medium; *lane 2*, strain CC-124 grown on zinc-deficient TAP medium; *lane 3*, strain 10-6C grown on TAP medium.

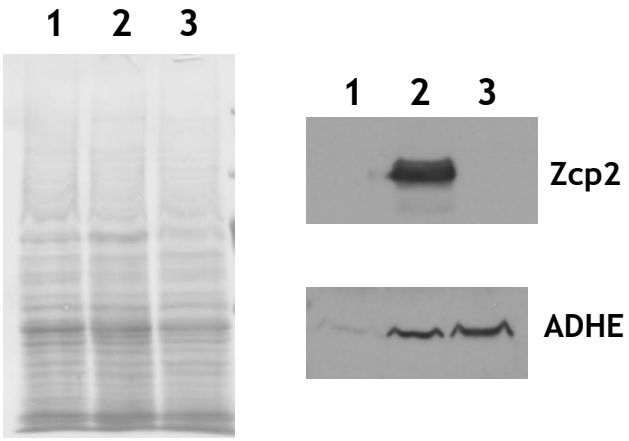

FIGURE S6. Production of antibodies to *Chlamydomonas* phosphotransacetylases
•**Protein Overexpression and Antibody Production-** A partial sequence of *C. reinhardtii PTA1* cDNA (coding for His^{492}–Asn^{778}; tPTA1) was amplified by PCR using oligonucleotide primers containing the EcoRI and HindIII restriction sites (underlined) as follows: 5′-GACGAATTCCACATCGTGCTGCCCGAGTC -3′, and 5′-GTCAAGCTTGTCGTTCACCGGCTTGAGCAG -3′. The PCR product was cloned in pGEM-T Easy (Promega) and recloned in the BamHI/HindIII sites of the overexpression vector pET24a (Novagen). The resultant construct was introduced in *Escherichia coli* strain BL21 to produce the recombinant protein. His-tagged protein was purified under denaturing conditions using Ni-NTA matrix (Qiagen), as recommended by the supplier. Antibodies against tPTA1 were produced at Eurogentec (Leuven, Belgium).

•**Specificity of the produced antibodies-** In a fraction enriched in *Chlamydomonas* chloroplasts, the anti-PTA1 serum recognized two bands, which likely correspond to the two phosphotransacetylases PTA1 and PTA2 present in the alga.

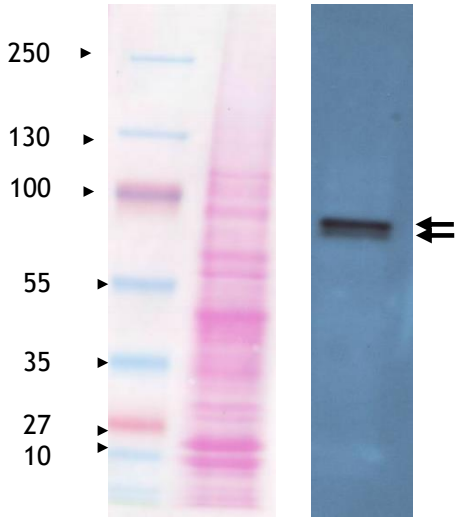

Anti-PTA
(1/2,000)

FIGURE S7. Identification of *Chlamydomonas* PTAs by mass spectrometry.

•**Urea/SDS-PAGE loaded with a fraction enriched in chloroplasts.** Chloroplasts were isolated from strain 10-6C and loaded on a urea/SDS-PAGE. The gel piece that contained the protein detected by the anti-PTA serum (see Supplemental Figure S6) was subjected to nanoLC-MS/MS analysis.

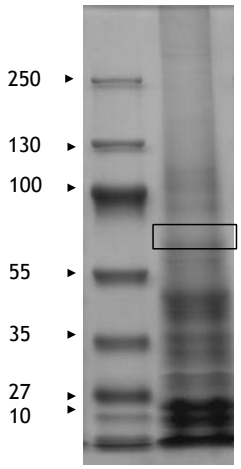

•Identification of PTAs by mass spectrometry

	accession	score	mass	coverage	#peptides	emPAI
PTA2	Cre09.g396650.t1.1	2215,23	85020,14	54,58	29	3,56
PTA1	Cre17.g699000.t1.1	1977,00	86071,30	50,12	28	2,24

Tryptic peptides that match *Chlamydomonas* PTAs. Peptides that match chloroplast PTA2 protein are highlighted in green; tryptic peptides that match mitochondrial PTA1 protein are highlighted in yellow. The underlined sequence correspond to tPTA1 used for antibody production (See Supplemental Figure 3).

```
PTA2      MSLNSSTMSRRQ---A-VAGAPAVAPFRHAGLFPRVRLCANRRVARVAP-KAAGNGNIAQ
PTA1      MAFASSSMAALSRPLAAVSSGLGSALSRASQLLTSGSLSSSPTASHSSTRRFISDG-TVG
          *:: **:*:  .   * *:.. . *  * : *:    *.:.  .:: :  :  .:*  .

PTA2      GEQGFDTLFLSDISLVGQRTPLLLGFFNYFERHLPHVGFFEPIAAEALASSELRIDRHVE
PTA1      SKGRPDSLFLSDISMSGHRAPLLLGWLNYLERHLPHVGFFEPIGGRALAGSELSVDRHVE
          .:   *:*******: *:*:*****::**:*************...***.*** :*****

PTA2      LVYKVFNLKGDVRAMTGVQDAEAARMIANGQHSELLDKIYSQYASYKEGQ--DLVLVEGP
PTA1      LMYRVFNMKGDATRMTGISDTEAAQLIASGKQSEVLDRIYAAYMAYKAGGELDLCLVEGP
          *:*:***:***.  ***:.*:***::**.*::**:**:**: * :** *   ** *****

PTA2      GPLMGGTELDAQIAAALNAPVLMTMTGQPNATVADYYNRAMVKRQVFLDHHVEVLGLVMN
PTA1      GPLMGGTELDAQIAAALNAPVLMAMSGRPNATANDYYNKAMVKRQVFADHKVDVLGVVIN
          **********************:*:*:****. ****:******** **:*:***:*:*

PTA2      GLPRQSHAILSGQLRDKFAAAGLPFAGAIPTDIMLRNVRLDEVQTAMGAQRLYGDSLLTD
PTA1      GLPREHHAILSSQLRDKLERAGLPFAGALPEDPVLSSVRLDEVRTALGATQLYGETWLGD
          ****: *****.*****:  ********:* * :* .******:**:** :***:: * *
```

```
PTA2      VEFDDVVVASQRLEELLEILAERPMGRPLVVTSADRLDIVLGLLAAQLSVSGPGVAGILL
PTA1      VEFDEVVVGSQRLEELLETLVERPMGRPLVVTSADRLDIVLGLLAAQLSVRGPSVAGVLL
          ****:***.********* *.**************************** **.***:**

PTA2      TQAGSARSGRNYARDTIDRIFAGLSS-------------------SGLYKGSLLPVLVT
PTA1      TQAGASRITRSYAKSAVDNIFAGLSNNTGASGGGPDGAAAANGSAQGSLYRGALLPVLST
          ****::*  *.**:.::*.******.                    ..**:*:***** *

PTA2      DMPLRDAIRKLDNLDAAILPSSTRKISQCKRLFEQYVDANAVVARLQNMVRPNRMTPKMF
PTA1      DKHLAEALAVIGRMDASILPTSIRKVTQCKMLFDKYIDANAVVTGLQK-SRPTRVTPKMF
          *  * :*:  : .:**:***:* **::*** **::*:******: **:  **.*:*****

PTA2      MHTLKSMCNATPQHIVLPESEDKRVLAAAADVVQRGLAKITLLGDPTTILAEAAKLGLDL
PTA1      QHTMKAMCRASPQHIVLPESVDKRVLAAAADVTARGLARVTLLGDPTTVQAEAKKLGLDL
           **:*:**.*:********* **********. ****::********: *** ******

PTA2      SGCNIHNPNTSDRFDKYVDMLVEARKKKGMTREVAADTLHGDVNFFATMMIVAGDADGMV
PTA1      SGCHIHNPNSSDRFDKYVDMLVEARKKKGMTREAAADTLHGDINFFGTMMVAAGDADGMV
          ***.*****:**********************.********:***.***:.********

PTA2      SGAVHTTASTVRPALQVLKSPDTPLVSSVFIMCLPDRVVVYGDCAVNVNPSAADLAQIAI
PTA1      SGAIHTTASTIRPALQMLKNPASSLVSSIFFMCLPDRVLVYGDCAVNVSPSAADLAAIAT
          ***:******:*****:**.* : ****:*:*******:*********.******* **

PTA2      TSNDTAAAFGIEPRVAMLSYSTLGSGSGPDVQKVSEAVAIVKQRRPDIKVEGPIQYDAAI
PTA1      TSADTAAAFGIEPRVAMLSYSTLGSGAGPDVQKVTEAVALVKQQRQDIKVEGPIQYDAAI
          ** ************************:*******:****:***:* **************

PTA2      DPKVAAVKVQGLSEVAGKATVFIFPDLNTGNNTYKAVQQSTGAIAMGPVMQGLLRPVNDL
PTA1      DPAVAAVKVKGGSEVAGRATVFVFPDLNTGNNTYKAVQQSTGAIAMGPVMQGLLKPVNDL
          ** ******:* *****:****:*********************************:*****

PTA2      SRGCTVPDIINTICVTSIQASRMSSAARAAAAKAAVAAV*
PTA1      SRGCTVPDIVNTICVTSIQAMQFKQRTQAAVAAAAAPK*-
          *********:********** ::.. ::**.* **.
```